EUROPEAN ORGANIZATION FOR NUCLEAR RESEARCH (CERN)

CERN-PH-EP-2010-003
05 Feb 2010

CMS-QCD-09-010

Transverse-momentum and pseudorapidity distributions of charged hadrons in pp collisions at $\sqrt{s}$ = 0.9 and 2.36 TeV

The CMS Collaboration*

Abstract

Measurements of inclusive charged-hadron transverse-momentum and pseudorapidity distributions are presented for proton-proton collisions at $\sqrt{s} = 0.9$ and 2.36 TeV. The data were collected with the CMS detector during the LHC commissioning in December 2009. For non-single-diffractive interactions, the average charged-hadron transverse momentum is measured to be 0.46 ± 0.01 (stat.) $\pm$ 0.01 (syst.) GeV/c at 0.9 TeV and 0.50 ± 0.01 (stat.) $\pm$ 0.01 (syst.) GeV/c at 2.36 TeV, for pseudorapidities between -2.4 and $+2.4$. At these energies, the measured pseudorapidity densities in the central region, $dN_{\rm ch}/d\eta|_{|\eta|<0.5}$, are 3.48 ± 0.02 (stat.) $\pm$ 0.13 (syst.) and 4.47 ± 0.04 (stat.) $\pm$ 0.16 (syst.), respectively. The results at 0.9 TeV are in agreement with previous measurements and confirm the expectation of near equal hadron production in $\mathrm{p\bar{p}}$ and pp collisions. The results at 2.36 TeV represent the highest-energy measurements at a particle collider to date.

*See Appendix A for the list of collaboration members

1 Introduction

Measurements of transverse-momentum (p_T) and pseudorapidity (η) distributions are reported for charged hadrons produced in proton-proton (pp) collisions at centre-of-mass energies ($\sqrt{s}$) of 0.9 and 2.36 TeV at the CERN Large Hadron Collider (LHC) [1]. The data were recorded with the Compact Muon Solenoid (CMS) experiment in December 2009 during two 2-hour periods of the LHC commissioning, demonstrating the readiness of CMS in the early phase of LHC operations. The results at $\sqrt{s} = 2.36$ TeV represent the highest-energy measurements at a particle collider to date.

The majority of pp collisions are soft, i.e., without any hard scattering of the partonic constituents of the proton. In contrast to the higher-p_T regime, well described by perturbative QCD, particle production in soft collisions is generally modelled phenomenologically to describe the different pp scattering processes: elastic scattering, single-diffractive and double-diffractive dissociation, and inelastic non-diffractive scattering [2].

The measurements presented in this paper are the inclusive primary charged-hadron multiplicity densities (dN_{ch}/dp_T and $dN_{ch}/d\eta$) in the pseudorapidity range $|\eta| < 2.4$, where p_T is the momentum of the particle transverse to the beam axis, and where N_{ch} is the number of charged hadrons in any given η or p_T interval. The pseudorapidity η is defined as $-\ln[\tan(\theta/2)]$, where θ is the polar angle of the particle with respect to the anti-clockwise beam direction.

Primary charged hadrons are defined as all charged hadrons produced in the interactions, including the products of strong and electromagnetic decays, but excluding products of weak decays and hadrons originating from secondary interactions. In this paper, the multiplicity densities are measured for inelastic non-single-diffractive (NSD) interactions to minimize the model dependence of the necessary corrections for the event selection, and to enable a comparison with earlier experiments. The event selection was therefore designed to retain a large fraction of inelastic double-diffractive (DD) and non-diffractive (ND) events, while rejecting all elastic and most single-diffractive dissociation (SD) events.

Measurements of dN_{ch}/dp_T and $dN_{ch}/d\eta$ distributions and their $\sqrt{s}$ dependence are important for understanding the mechanisms of hadron production and the relative roles of soft and hard scattering contributions in the LHC energy regime. Furthermore, the measurements at the highest collision energy of 2.36 TeV are a first step towards understanding inclusive particle production at a new energy frontier. These measurements will be particularly relevant for the LHC as, when it is operated at design luminosity, rare signal events will be embedded in a background of more than 20 near-simultaneous minimum-bias collisions. These results will also serve as a reference in the measurement of nuclear-medium effects in PbPb collisions at the LHC. The differences in these distributions between pp and $p\bar{p}$ collisions are expected to be smaller than the attainable precision of these measurements [3]. The results reported here at $\sqrt{s} = 0.9$ TeV can therefore be directly compared to those previously obtained in $p\bar{p}$ collisions.

This paper is organized as follows. In Section 2, the elements of the CMS detector relevant to this analysis are outlined. In Sections 3 and 4, the event selection and reconstruction algorithms are described. Results on dN_{ch}/dp_T and $dN_{ch}/d\eta$ are presented in Section 5 and compared with previous $p\bar{p}$ and pp measurements in Section 6.

2 The CMS detector

A detailed description of the CMS experiment can be found in Ref. [4]. The central feature of the CMS apparatus is a superconducting solenoid of 6 m internal diameter, providing a

uniform magnetic field of 3.8 T. Immersed in the magnetic field are the pixel tracker, the silicon-strip tracker (SST), the lead-tungstate crystal electromagnetic calorimeter (ECAL) and the brass/scintillator hadron calorimeter (HCAL). In addition to barrel and end-cap detectors for ECAL and HCAL, the steel/quartz-fibre forward calorimeter (HF) covers the region of $|\eta|$ between 2.9 and 5.2. The HF tower segmentation in η and azimuthal angle ϕ (expressed in radians) is 0.175×0.175, except for $|\eta|$ above 4.7 where the segmentation is 0.175×0.35. Muons are measured in gas-ionization detectors embedded in the steel return yoke.

The tracker consists of 1440 silicon-pixel and 15 148 silicon-strip detector modules and measures charged particle trajectories within the nominal pseudorapidity range $|\eta| < 2.5$. The pixel tracker consists of three 53.3 cm long barrel layers and two end-cap disks on each side of the barrel section. The innermost barrel layer has a radius of 4.4 cm, while for the second and third layers the radii are 7.3 cm and 10.2 cm, respectively. The tracker is designed to provide an impact-parameter resolution of about 100 μm and a transverse-momentum resolution of about 0.7 % for 1 GeV/c charged particles at normal incidence (η=0) [5].

During the data-taking period addressed by this analysis, 98.4% of the pixel and 97.2% of the SST channels were operational. The fraction of noisy pixel channels was less than 10^{-5}. The signal-to-noise ratio in the SST depends on the sensor thickness and was measured to be between 28 and 36, consistent with the design expectations and cosmic-ray measurements [5, 6]. The tracker was aligned as described in Ref. [7] using cosmic ray data prior to the LHC commissioning. The precision achieved for the positions of the detector modules with respect to particle trajectories is 3-4 μm in the barrel for the coordinate in the bending plane.

Two elements of the CMS detector monitoring system, the Beam Scintillator Counters (BSCs) [4, 8] and the Beam Pick-up Timing for the eXperiments (BPTX) devices [4, 9], were used to trigger the detector readout. The two BSCs are located at a distance of $\pm$10.86 m from the nominal interaction point (IP) and are sensitive in the $|\eta|$ range from 3.23 to 4.65. Each BSC is a set of 16 scintillator tiles. The BSC elements have a time resolution of 3 ns and an average minimum-ionizing-particle detection efficiency of 96.3%, and are designed to provide hit and coincidence rates. The two BPTX devices, located around the beam pipe at a distance of $\pm$175 m from the IP on either side, are designed to provide precise information on the bunch structure and timing of the incoming beam, with better than 0.2 ns time resolution.

The CMS experiment uses a right-handed coordinate system, with the origin at the nominal interaction point, the x axis pointing to the centre of the LHC, the y axis pointing up (perpendicular to the LHC plane) and the z axis along the anticlockwise-beam direction. The azimuthal angle, ϕ, is measured in the (x,y) plane, where $\phi = 0$ is the $+x$ and $\phi = \pi/2$ is the $+y$ direction.

The detailed Monte Carlo (MC) simulation of the CMS detector response is based on Geant4 [10]. The position and width of the beam spot in the simulation were adjusted to that determined from the data. Simulated events were processed and reconstructed in the same manner as collision data.

3 Event selection

This analysis uses two LHC collision data sets collected with pp interaction rates of about 11 and 3 Hz at $\sqrt{s} = 0.9$ and 2.36 TeV, respectively. At these rates, the probability for more than one inelastic collision to occur in the same proton bunch crossing is less than 2×10^{-4} at both collision energies.

Events were selected by a trigger signal in any of the BSC scintillators, coincident with a sig-

nal from either of the two BPTX detectors indicating the presence of at least one proton bunch crossing the IP. From these samples, collision events were selected offline by requiring BPTX signals from both beams passing the IP and at least one reconstructed charged particle trajectory in the pixel detector originating from within 0.2 cm of the beam position in the transverse direction (Section 4.1). The total number of collision events and the numbers of collision events passing each requirement are listed in Table 1.

Table 1: Numbers of events per data sample used in this analysis. The offline event selection criteria are applied in sequence, i.e., each line includes the selection of the lines above.

Centre-of-mass Energy	0.9 TeV	2.36 TeV
Selection	Number of Events	
BPTX Coincidence + one BSC Signal	72 637	18 074
One Pixel Track	51 308	13 029
HF Coincidence	40 781	10 948
Beam Halo Rejection	40 741	10 939
Beam Background Rejection	40 647	10 905
Valid Event Vertex	40 320	10 837

To select NSD events, a coincidence of at least one HF calorimeter tower with more than 3 GeV total energy on each of the positive and negative sides of the HF was required. Events containing beam-halo muons crossing the detector were identified by requiring the time difference between any two hits from the BSC stations on opposite sides of the IP to be within 73 ± 20 ns. Such events were removed from the data sample. Beam-induced background events producing an anomalously large number of pixel hits were excluded by rejecting events with pixel clusters (Section 4.2) inconsistent with a pp collision vertex. This rejection algorithm was only applied for events with more than 150 pixel clusters, providing a clean separation between collision events and beam background events. Finally, events were required to contain at least one reconstructed primary vertex, as described in Section 4.

To study beam-induced background, the event selection criteria were also applied to a data sample obtained by selecting events with only a single unpaired bunch crossing the IP. The contamination of background events in the colliding-bunch data sample was estimated by taking into account the total unpaired and paired bunch intensities and was found to be negligible ($<$0.1%). The total number of cosmic-ray muons in the selected data sample was estimated to be less than one event, and was also neglected.

The event selection criteria are expected to have high efficiency for the NSD part of the pp cross section, while rejecting a large fraction of the SD component of pp interactions. The efficiency of the event selection for the different processes and centre-of-mass energies was determined using simulated events obtained from the PYTHIA [11] (version 6.420, tune D6T, [12]) and PHOJET [13, 14] (version 1.12-35) event generators processed with a MC simulation of the CMS detector response (hereafter simply called PYTHIA and PHOJET). In the case of PHOJET, the discussion and numerical values concerning the DD process given in this paper contain both the DD and the Double-Pomeron-Exchange (DPE) processes. The relative event fractions of SD, DD and ND processes and event selection efficiencies at $\sqrt{s} = 0.9$ and 2.36 TeV are listed in Table 2 for these two samples.

The measurements were corrected for the selection efficiency of NSD processes and for the fraction of SD events contained in the data sample after the event selection. Based on the

PYTHIA (PHOJET) event generator, the fractions of SD events contained in the selected data samples were estimated to be 5.2% (4.9%) at 0.9 TeV and 6.3% (5.0%) at 2.36 TeV.

Table 2: Expected fractions of SD, DD, ND and NSD processes ("Frac.") obtained from the PYTHIA and PHOJET event generators before any selection and the corresponding selection efficiencies ("Sel. Eff.") determined from the MC simulation.

	PYTHIA				PHOJET			
Energy	0.9 TeV		2.36 TeV		0.9 TeV		2.36 TeV	
	Frac.	Sel. Eff.	Frac.	Sel. Eff.	Frac.	Sel. Eff.	Frac.	Sel. Eff.
SD	22.5%	16.1%	21.0%	21.8%	18.9%	20.1%	16.2%	25.1%
DD	12.3%	35.0%	12.8%	33.8%	8.4%	53.8%	7.3%	50.0%
ND	65.2%	95.2%	66.2%	96.4%	72.7%	94.7%	76.5%	96.5%
NSD	77.5%	85.6%	79.0%	86.2%	81.1%	90.5%	83.8%	92.4%

The generated charged-hadron multiplicity distribution is shown in Fig. 1a in the range $|\eta| < 2.5$ for all inelastic events after event selection. The event selection efficiency for NSD events is shown in Fig. 1b as a function of generated charged-hadron multiplicity in the region $|\eta| < 2.5$. The correction for the event selection efficiency was applied as a function of number of reconstructed charged particles per event, as illustrated at generator level in Figs. 1a and 1b.

The sum of the corrections to the $dN_{\mathrm{ch}}/d\eta$ measurements due to the NSD event selection efficiency and the SD event contamination typically amounts to 8%. The corrections applied in the analysis are based on PYTHIA using the default SD and DD process fractions as listed in Table 2.

The PYTHIA predictions for the SD and DD fractions differ from those of PHOJET, and are not fully consistent with existing measurements, as explained in Section 5. These differences propagate to a systematic uncertainty of 2% in the $dN_{\mathrm{ch}}/d\eta$ measurement. To estimate the additional systematic uncertainty on the event selection efficiency correction resulting from the possible inaccuracies in the detector simulation, the analysis was repeated after replacing the HF event-selection criterion with a two-sided hit coincidence of signals in the BSC detectors. Based on this comparison, an additional 1% systematic uncertainty was assigned to the $dN_{\mathrm{ch}}/d\eta$ measurements.

4 Reconstruction algorithms

The analysis presented in this paper measures the $dN_{\mathrm{ch}}/d\eta$ and $dN_{\mathrm{ch}}/dp_{\mathrm{T}}$ distributions of primary charged hadrons. The $dN_{\mathrm{ch}}/d\eta$ distributions were obtained using three methods based on counting of (i) reconstructed clusters in the pixel barrel detector; (ii) pixel tracklets composed of pairs of clusters in different pixel barrel layers; and (iii) tracks reconstructed in the full tracker volume, combining the pixel and strip hits. The cluster counting method provides an independent measurement for each pixel barrel layer, and the tracklet method for each pair of layers. The third method also allows a measurement of the $dN_{\mathrm{ch}}/dp_{\mathrm{T}}$ distribution. All three methods rely on the reconstruction of the primary vertex (PV) described in Section 4.1.

The pixel-cluster-counting method has the advantage of having the largest p_T acceptance down to small transverse momentum (30 MeV/c), is insensitive to geometrical misalignment of the detector and does not require detailed knowledge of the primary vertex position resolution. A potential disadvantage is the sensitivity to backgrounds from collisions with residual gas in

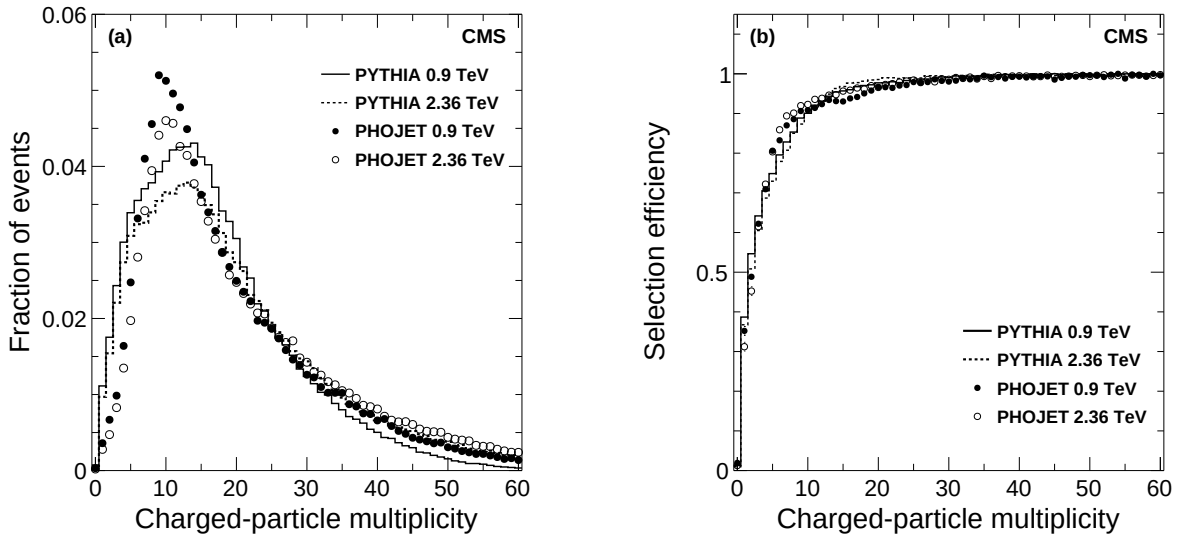

Figure 1: (a) Generated multiplicity distributions of primary charged hadrons in the range $|\eta| < 2.5$ for $\sqrt{s} = 0.9$ TeV (solid dots and histogram) and 2.36 TeV (open circles and dashed histogram) after the event selection is applied to the reconstructed events, using inelastic events from the PYTHIA (histograms) and PHOJET (symbols) event generators. (b) The event selection efficiency expected for NSD events from the PYTHIA (histograms) and PHOJET (symbols) event generators as a function of generated charged hadron multiplicity in the region $|\eta| < 2.5$.

the beam pipe (beam-gas collisions), from secondary particles produced in the detector material and from low-p_T particles curling in the axial magnetic field (loopers). The pixel-tracklet method is capable of measuring and correcting for the combinatorial background and has a p_T threshold of 50 MeV/c. The third method uses the tracker (pixel and SST) to build tracks. It requires at least two pixel hits in different layers, has the largest p_T threshold ($\approx$100 MeV/c) and algorithmic complexity, but is the most robust against background hits produced by particles not originating from the collision. The charged-particle multiplicity was corrected in all three methods for the small contamination ($< 1\%$) of primary charged leptons. The measured $dN_{ch}/d\eta$ values were evaluated by extrapolating or correcting to $p_T = 0$ for all the three analysis methods.

The three reconstruction methods are described in Sections 4.2- 4.4.

4.1 Primary vertex reconstruction

The x, y and z positions of the luminous region where protons of both beams interact, hereafter referred to as beam spot, are obtained for each data set from three-dimensional vertex fits based on tracks reconstructed with $p_T > 0.9\,\mathrm{GeV/c}$, using the full event sample. The RMS of the beam spot in the transverse directions was found to be less than 0.05 cm. The beam spot position and dimensions were found to be stable within a given data set.

To reconstruct the z coordinate of the PV for each event, tracks consisting of triplets of pixel hits were formed. The minimum transverse momentum of these tracks is $\approx$ 75 MeV/c. The tracks were required to originate from the vicinity of the beam spot with a transverse impact parameter (d_T) smaller than 0.2 cm. Of these tracks, only those with $d_T < 4\,\sigma_T$, where σ_T is the quadratic sum of the uncertainty in d_T and the RMS of the beam spot in the transverse

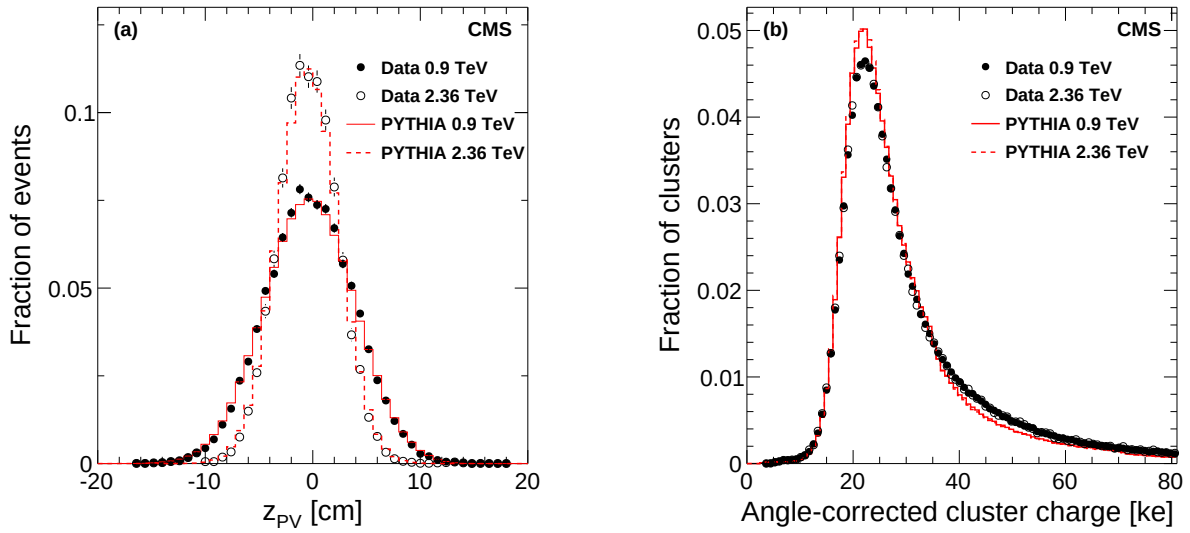

Figure 2: (a) The distribution of the reconstructed z position of the primary vertex in the data (dots), compared to that from the PYTHIA simulation (histogram). (b) Distribution of the cluster charge multiplied by $|\sin\theta|$ in the data (dots) and the simulation (histogram), for the clusters selected for analysis.

direction, were used in the vertex reconstruction.

The vertex-reconstruction algorithm uses the z coordinate of the tracks at the point of closest approach to the beam axis and the corresponding estimated measurement uncertainty (σ_z). It performs an agglomerative clustering by adding tracks to form groups. These groups (denoted the i^{th} and j^{th} group) are then merged based on their normalized distance, $d_{ij}^2 = (z_i - z_j)^2/(\sigma_i^2 + \sigma_j^2)$ where σ_i and σ_j are the uncertainties of the z_i and z_j positions, with a fast nearest-neighbour search algorithm [15]. The z position and its uncertainty σ_z for the newly joined group are calculated using a weighted average. The clustering process stops when the smallest normalized distance between the remaining groups gets larger than 8.0, where the stopping condition was optimized using simulated events. Only vertices formed from at least two tracks were considered except when only one track was reconstructed in the event. In the latter case the PV position was defined as the point of the closest approach of the track to the beam axis. The fraction of single-track vertices in the selected data sample is 1.7% (1.3%) at 0.9 TeV (2.36 TeV). The overall PV reconstruction efficiency, evaluated from the data after all other event selection cuts, is in excess of 99% and the fraction of events with more than one primary vertex candidate is 5.0% (7.4%) at 0.9 TeV (2.36 TeV). In the rare case of multiple PV candidates, the vertex composed of the largest set of tracks was chosen.

The reconstructed primary vertex resolution in the z direction is a function of the associated track multiplicity (N) and was found to be parameterized adequately as 0.087 cm $/N^{0.6}$ using simulated events.

The distribution of the reconstructed z position of the PV is shown in Fig. 2a. Overlaid is the PV distribution in simulated events, the position and RMS of which were adjusted to reproduce the beam spot measured in data.

4.2 Pixel cluster counting method

The pseudorapidity distribution of primary charged hadrons produced in a pp collision can be measured by counting the number of clusters they create when traversing each of the three pixel barrel layers and applying appropriate corrections, as described in this section.

The energy deposited by charged particles traversing a pixel detector layer is spread over multiple pixels. Adjacent pixels with a charge measurement above a readout threshold of typically 2740 electrons are combined into pixel clusters to integrate the total charge deposit [6]. The cluster size and charge depend on the incident angle of the particle with respect to the active detector surface. The cluster length along the z axis ranges from 1-2 pixels at normal incident angle up to 14-16 pixels at shallow crossing angles. Figure 2b shows the measured distribution of cluster charge multiplied by $|\sin\theta|$ (or $1/\cosh\eta$) after the cluster selection discussed below, compared to the simulation. Here, θ is the polar angle of the straight line connecting the PV to the cluster.

The peak position is consistent with the expected charge of 22 ke, while the width of the distribution is slightly larger in the data than in the simulation due to gain calibration non-uniformities.

The cluster counting method correlates the observed pixel-cluster length in the z direction, expressed in number of pixels, with the expected path length traveled by a primary particle at a given η value. For primary particles the cluster length in z is proportional to $|\cot\theta|$ (or $|\sinh\eta|$) as displayed in Fig. 3a. Small clusters at large $|\eta|$ are due to loopers, secondary particles and daughters of long-lived hadrons. Clusters from these background particles were efficiently removed by the cluster-length cut represented by the solid line in Fig. 3a. To allow for an efficient background rejection, only the barrel part of the pixel detector was used, where the detector units are parallel to the beam axis, as opposed to the pixel end-caps. Furthermore, the η range for the cluster counting was restricted to $|\eta| < 2$ to avoid acceptance problems due to the slightly off-centred position of the luminous region.

The event selection efficiency and the SD contribution for a given total multiplicity of selected clusters (M) for each pixel barrel layer can be determined from Monte Carlo simulation. The overall change of the $dN_{\mathrm{ch}}/d\eta$ value due to this correction is 9% for both collision energies.

The fraction of clusters created by loopers above the cluster-length cut (1% and 5% for $\eta = 2$ and $\eta = 0.5$, respectively) can be estimated by measuring the total number of clusters below the cut in data, corrected by the ratio of looper clusters below and above the cut in simulated events. The number of clusters eliminated by the cluster-length cut was found to be higher in data than in simulated events by 10-20% due to a slightly larger abundance of secondary particles and loopers, while the observed number and length distributions of clusters above the cut was found to agree with the simulation.

The corrections for absorption in the beam pipe and detector material, secondary particles, daughters of long-lived hadrons, delta-ray electrons and double hits caused by geometrically overlapping detector units were all evaluated, in bins of η and M, with simulated data. The size of these corrections is 10%, 23% and 41% for the first, second and third detector layer, respectively. Varying the charged-particle multiplicity in the event generator by 50% only causes a $\pm 3\%$ relative change in these corrections. Their dependence on η and pixel-cluster multiplicity is similarly small.

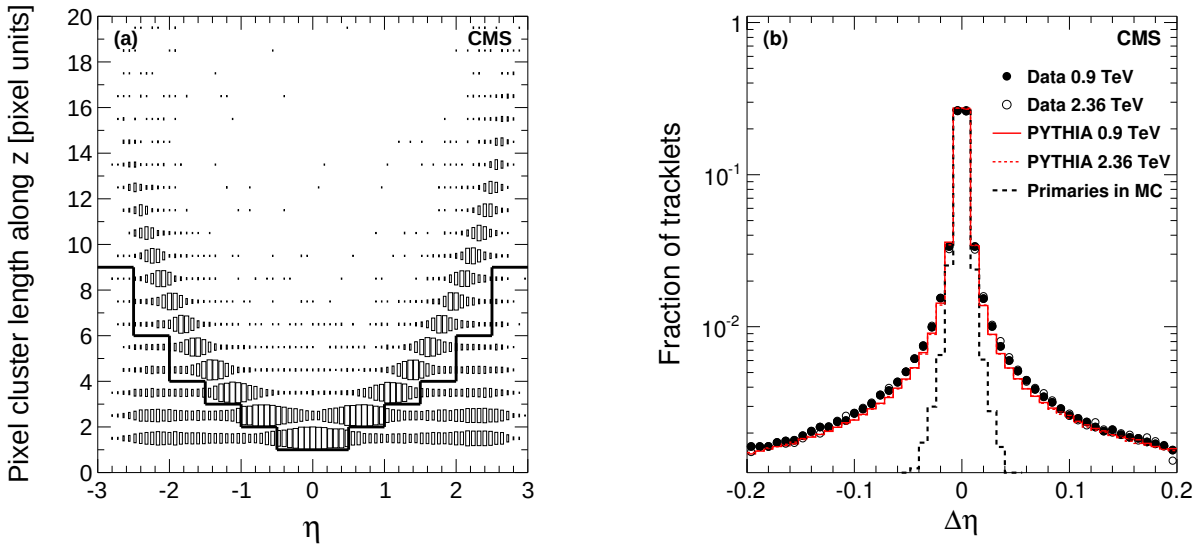

Figure 3: (a) Pixel cluster length along z as a function of η for the 900 GeV data. The solid line illustrates the cut applied in the cluster counting method. (b) The $\Delta\eta$ distribution of clusters on tracklets in the data (dots and circles), together with the distribution obtained from the PYTHIA simulation (solid and dotted lines), for both 0.9 and 2.36 TeV collision energy. The dashed line shows the $\Delta\eta$ distribution of clusters for primary charged-particle tracks in the Monte Carlo simulation at 0.9 TeV. The tail of the $\Delta\eta$ distribution comes from the combinatorial background.

4.3 Pixel-tracklet method

This method was first used to measure charged-hadron multiplicities by the PHOBOS experiment at RHIC [16]. Pixel tracklets are constructed from combinations of two pixel hits in any two pixel barrel layers. The difference in the angular positions of the two clusters with respect to the PV, $\Delta\eta$ and $\Delta\phi$, are calculated for each tracklet. If two tracklets share a hit, the tracklet with the larger $\Delta\eta$ is discarded. The $\Delta\eta$ distribution of reconstructed tracklets is shown in Fig. 3b, together with the corresponding distribution from simulated data and a separate distribution for simulated primary particles only. Tracklets from primary particles display a sharp peak at $\Delta\eta = 0$, while the tracklets from the combinatorial background have an extended tail. The simulated $\Delta\eta$ distributions are in good agreement with data.

To suppress the combinatorial background, only tracklets with $|\Delta\eta| < 0.1$ and $|\Delta\phi| < 1.0$ were selected. Since the combinatorial background is flat in $\Delta\phi$, the remaining fraction of background tracklets in the signal region $|\Delta\phi| < 1.0$ can be estimated from tracklets with $1.0 < |\Delta\phi| < 2.0$. This data-driven estimate of the background accurately describes the raw $\Delta\eta$ distribution of tracklets for $|\Delta\eta| > 2$, where no signal from primary particles is expected from the MC simulation. Typical values of this estimated background fraction in the signal region increase with $|\eta|$ from 2% to 30%. The η range for the tracklet method was restricted to $|\eta| < 2$ to avoid a large acceptance correction.

The contribution from secondary particles, reconstruction efficiency and geometrical acceptance needs to be accounted for to determine the number of primary charged hadrons. These correction factors were calculated using PYTHIA simulations for background-subtracted tracklets in bins of z position of the PV, pseudorapidity, and tracklet multiplicity. The magnitude of the correction varies with $|\eta|$ from 0 to 20%. The correction factors were also cross-checked by PHOJET simulations and only cause a 2-3% change in the $dN_{\mathrm{ch}}/d\eta$ result.

The correction for the event selection efficiency and the SD contribution was determined for each tracklet multiplicity bin. The overall change in the $dN_{\rm ch}/d\eta$ value due to this correction is about 8% at $\eta = 0$.

4.4 Tracking method

Pixel and SST detectors were used to reconstruct tracks, including both barrel and end-cap layers. The acceptance was limited to $|\eta| < 2.4$ to avoid edge effects. The iterative reconstruction procedure described below follows Refs. [17, 18], but was further optimized for primary-track reconstruction in minimum bias events.

In the first step of track reconstruction, tracks with three pixel hits (triplets) are built using the x and y positions of the beam spot and the z coordinate of the primary vertex as constraints. These clean pixel tracks are used as seeds for the Kalman-filter-based trajectory-building algorithm in the SST. The resulting trajectories are stored. Before the second tracking step, the pixel and strip hits associated with the tracks found in the first step are removed from further consideration. The second step uses pixel triplet seeds as well, but does not require a vertex constraint and has a looser transverse impact parameter requirement than in the first step. After removal of hits associated with tracks found in the second step, the third tracking step finds primary tracks seeded by two hits in the pixel detector. At least three hits were required for a track to be accepted.

Tracks found during the three iterative steps were collected and a second iteration of the PV reconstruction, as described in Section 4.1, was performed to refine primary vertex position determination. Finally, the tracks were refit with the corresponding vertex constraint, thus improving their η and $p_{\rm T}$ resolution.

In this analysis, a reconstructed track was considered as a primary-track candidate if it is compatible with originating from the PV ($d_{\rm T} < \min(4\sigma_{\rm T}, 0.2\,{\rm cm})$ and $d_z < 4\sigma_z$, where d_z is the distance between the point of the closest approach of the track to the beam axis and the PV along the z direction).

Studies with simulated events showed that the combined geometrical acceptance and reconstruction efficiency for the tracking method exceeds 50% around $p_{\rm T} \approx 0.1$, 0.2 and 0.3 GeV/c for pions, kaons and protons, respectively. The efficiency is about 96% in the $|\eta| < 1$ region for $p_{\rm T} > 0.25$ GeV/c, and is above 80% for pions at $p_{\rm T} = 0.15$ GeV/c. By requiring the geometrical shapes of the pixel clusters to be consistent with the crossing angle and direction of the track, the fraction of fake tracks was kept below 1%. The fraction of duplicated tracks (e.g., from loopers) was estimated to be about 0.1% in the central region, rising to 0.5% at large $|\eta|$.

The measured yield in data was corrected, based on MC simulation and comparisons with data, for geometrical acceptance (2% correction for $p_T > 200$ MeV/c), efficiency of the reconstruction algorithm (5-10% for $p_T > 300$ MeV/c), fake and duplicate tracks (<1% each). The contamination of less than 2% from decay products of long-lived hadrons, photon conversions and inelastic hadronic interactions with the detector material was also subtracted. To obtain the $dN_{\rm ch}/d\eta$ result from the $p_{\rm T}$ spectrum, an extrapolation to $p_{\rm T} = 0$ was necessary, resulting in an increase of 5% in the estimated number of charged hadrons.

Corrections based on the average hit efficiency of pixel layers, size of the beam spot, longitudinal and transverse impact-parameter resolutions of pixel tracks were validated with data. As an example, the average number of pixel and strip hits found on tracks in the range $|\eta| < 1$ is shown in Figs. 4a and 4b, together with the expectation from PYTHIA. Somewhat fewer particles are predicted with $p_T < 500$ MeV/c than seen in the data, which results in the small

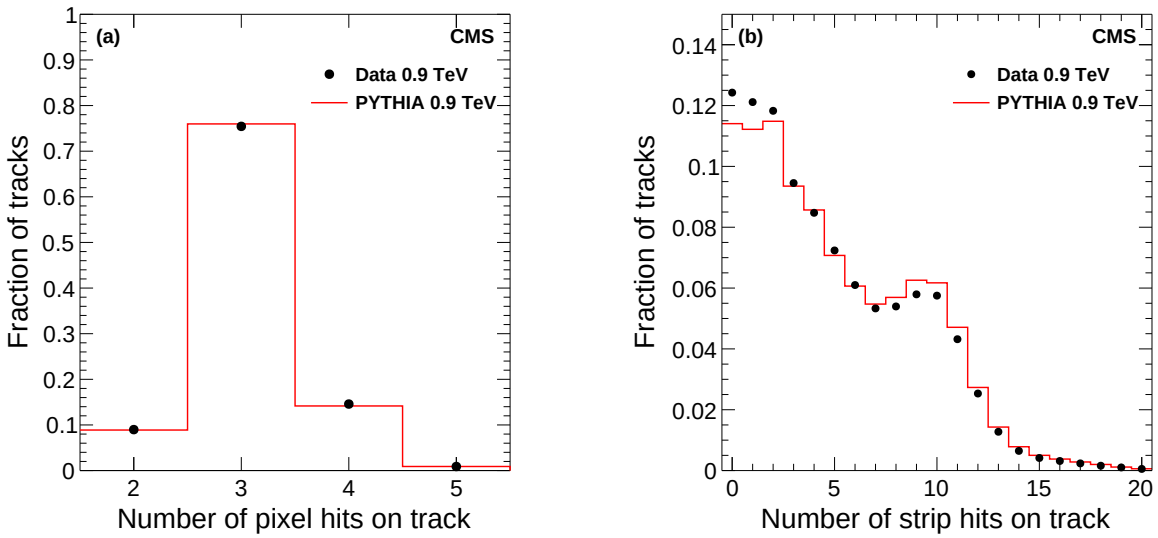

Figure 4: (a) The distribution of the number of pixel hits attached to reconstructed tracks in the region of $|\eta| < 1$ (closed circles), compared to the CMS detector simulation (histogram). (b) The distribution of the number of hits in the SST detector attached to reconstructed tracks in the region of $|\eta| < 1$ (closed circles), compared to the CMS detector simulation (histogram).

difference in the number of tracks with few SST hits in Fig. 4b. This small difference, which originates from limitations of the PYTHIA generator, does not affect the final measurement. The correction for the event selection efficiency and the SD contribution was determined for each track multiplicity bin, and has an overall magnitude of 8.3%.

5 Results

5.1 Systematic uncertainties

Various corrections and their event-selection and model dependence contribute to the systematic uncertainties of the measured quantities. A summary of these systematic uncertainties averaged over η and p_T is given in Table 3 and discussed below.

The uncertainties related to the trigger bias and to the event selection are common to all the analysis methods. The efficiency of the trigger and event-selection was corrected for by the prediction of the PYTHIA D6T event generator combined with the full Geant4 simulation of the CMS detector. The material description relevant for this analysis was verified by studies of photon conversion probabilities in the data, found to be in agreement with those obtained from the simulation.

Because single- and double-diffractive pp collisions have much smaller charged-hadron multiplicities per event than non-diffractive events, they contribute to the uncertainty in the measured $dN_{ch}/d\eta$ mostly through the uncertainty in the fraction of SD and DD events passing the event selection criteria. The fractions of SD events for $\sqrt{s} = 0.9$ TeV in PYTHIA and PHOJET (Table 2) are 23% and 19%, respectively. The UA5 experiment measured 15.5% for this fraction [19]. Based on the simulated trigger efficiencies for the different event types, only 5.5% of events passing the analysis event selection are expected to be single-diffractive events. From the aforementioned variations of SD fractions, an uncertainty of $\pm 1\%$ is attributed to this correction. The contribution of the uncertainty of the fraction of DD events was estimated sim-

ilarly to be $\pm 1\%$. Since underestimated DD and SD fractions both lead to an underestimated $dN_{\mathrm{ch}}/d\eta$ result, a conservative linear sum of 2% was assigned to the above systematic uncertainty. The trigger efficiency of the BSC is more than 98% for events with a valid vertex, and even a 5% uncertainty in single-particle detection efficiency of its individual segments results in a negligible uncertainty in the final result. The trigger efficiency of the BSC and the event selection efficiency of the HF detector were both measured from data and found to be consistent within 1% with the MC simulation. The total systematic uncertainty from propagating all event selection and trigger related uncertainties is 3%. The measurement of the average transverse momentum is less sensitive to the trigger selection efficiency. A smaller, 1% uncertainty was therefore assigned to that result.

The geometrical acceptance was studied by comparing the hit occupancy of the pixel barrel with the predictions from the simulation. The efficiency of the pixel hit reconstruction was estimated using tracks propagated from the SST to the pixel detector and by extrapolating pixel tracklets to the unused pixel barrel layer. The measured pixel hit efficiency was found to exceed 99% with a 0.5% uncertainty from both methods, which propagates into 0.5% uncertainty in the pixel-counting-based, 1% in the tracklet-based, and 0.3% in the track-based results. If the collected charge in one or more pixels in a cluster remains below the threshold, the cluster may be split. The splitting rate was estimated from the geometrical distance distributions of close-by pixel clusters found in the data and in the Monte Carlo simulation and found to be 0.5-0.9% in the simulation and 1.0-1.5% in data.

The uncertainty related to the cluster and tracklet selections was estimated by varying the selection cuts. An additional 3% and 2% uncertainty was assigned to the tracklet and track reconstruction algorithm efficiencies, respectively. Corrections for loopers and secondary particles are simulation dependent; the tracklet- and pixel-counting-based methods have low rejection power compared to the tracking method, thus carry a larger systematic uncertainty (as shown in Table 3).

The effects of the geometrical misalignment of the pixel barrel detector were simulated and a 1% uncertainty was assigned to the results from the tracklet-based method. Hits from beam-induced backgrounds coinciding with the collision were estimated to be very rare, and a conservative 1% random hit contribution was propagated to obtain the uncertainty of the results. The corrections for multiple track counting and fake track rate were estimated from the Monte Carlo simulation and found to be less than 1%. The uncertainty of the extrapolation to the full p_T-range depends on the low-p_T reach of the three methods and varies between 0.2 and 0.5%. While the sources of uncertainties are largely independent from each other, they are correlated among all the data points.

5.2 Charged hadron transverse-momentum distributions

Tracks with $|\eta| < 2.4$ and $p_{\mathrm{T}} > 0.1$ GeV/c were used for the measurement of $dN_{\mathrm{ch}}/dp_{\mathrm{T}}$. The measured average charged-hadron yields per NSD event are shown in Fig. 5a, as a function of p_{T} in bins of $|\eta|$. The yields were fit by the Tsallis function (Eq. 1), which empirically describes both the low-p_{T} exponential and the high-p_{T} power-law behaviours [20, 21]:

$$E\frac{d^3N_{\mathrm{ch}}}{dp^3} = \frac{1}{2\pi p_T}\frac{E}{p}\frac{d^2N_{\mathrm{ch}}}{d\eta dp_T} = C(n,T,m)\frac{dN_{\mathrm{ch}}}{dy}\left(1+\frac{E_T}{nT}\right)^{-n}, \quad (1)$$

where $y = 0.5\ln[(E+p_z)/(E-p_z)]$ is the rapidity; $C(n,T,m)$ is a normalization constant that depends on n, T and m; $E_{\mathrm{T}} = \sqrt{m^2+p_{\mathrm{T}}^2} - m$ and m is the charged pion mass. This function

Table 3: Summary of systematic uncertainties. While the various sources of uncertainties are largely independent, most of the uncertainties are correlated between data points and between the analysis methods. The event selection and acceptance uncertainty is common to the three methods and affects them in the same way. The values in parentheses apply to the $\langle p_T \rangle$ measurement.

Source	Pixel Counting [%]	Tracklet [%]	Tracking [%]
Correction on event selection	3.0	3.0	3.0 (1.0)
Acceptance uncertainty	1.0	1.0	1.0
Pixel hit efficiency	0.5	1.0	0.3
Pixel cluster splitting	1.0	0.4	0.2
Tracklet and cluster selection	3.0	0.5	-
Efficiency of the reconstruction	-	3.0	2.0
Correction of looper hits	2.0	1.0	-
Correction of secondary particles	2.0	1.0	1.0
Misalignment, different scenarios	-	1.0	0.1
Random hits from beam halo	1.0	0.2	0.1
Multiple track counting	-	-	0.1
Fake track rate	-	-	0.5
p_{T} extrapolation	0.2	0.3	0.5
Total, excl. common uncertainties	4.4	3.7	2.4
Total, incl. common uncert. of 3.2%	5.4	4.9	4.0 (2.8)

provides both the inverse slope parameter T, characteristic for low p_{T}, and the exponent n, which parameterizes the high-p_{T} power-law tail. These fit parameters change by less than 5% with η, thus a fit to the whole region $|\eta| < 2.4$ was performed. The p_{T} spectrum of charged hadrons, $1/(2\pi p_{\mathrm{T}}) d^2N_{\mathrm{ch}}/d\eta dp_{\mathrm{T}}$, in the region $|\eta| < 2.4$, was also fit with the empirical function (Eq. 1) and is shown in Fig. 5b. The p_{T} resolution of the CMS tracker was found to have a negligible effect on the measured spectral shape and was therefore ignored in the fit function. For the 0.9 TeV data, the inverse slope parameter and the exponent were found to be $T = 0.13 \pm 0.01$ GeV and $n = 7.7 \pm 0.2$. For the 2.36 TeV data, the values were $T = 0.14 \pm 0.01$ GeV and $n = 6.7 \pm 0.2$. The average transverse momentum, calculated from the measured data points adding the low- and high-p_{T} extrapolations from the fit is $\langle p_{\mathrm{T}} \rangle = 0.46 \pm 0.01$ (stat.) $\pm$ 0.01 (syst.) GeV/c for the 0.9 TeV and 0.50 ± 0.01 (stat.) $\pm$ 0.01 (syst.) GeV/c for the 2.36 TeV data.

The $dN_{\mathrm{ch}}/d\eta$ spectrum was obtained by summing the measured differential yields for $0.1 < p_{\mathrm{T}} < 3.5$ GeV/c and adding the result to the integral of the fit function for $p_{\mathrm{T}} < 0.1$ GeV/c and $p_{\mathrm{T}} > 3.5$ GeV/c. The latter term amounts to 5% of the total.

5.3 Charged hadron pseudorapidity density

The summary of results on the pseudorapidity density distribution of charged hadrons is shown in Fig. 6. The $dN_{\mathrm{ch}}/d\eta$ results for the three layers in the cluster-counting method and the three layer-pairs in the pixel-tracklet method are consistent within 3%. These results from the various layers and from the different layer pairs were combined to provide one set of data from each analysis method, as shown in Fig. 6a. The error bars include the systematic uncertainties of about 2.4–4.4% specific to each method, estimated from the variations of model parameters in the simulation used for corrections and the uncertainties in the data-driven corrections. The systematic uncertainties common to all the three methods, which amount to 3.2%, are not

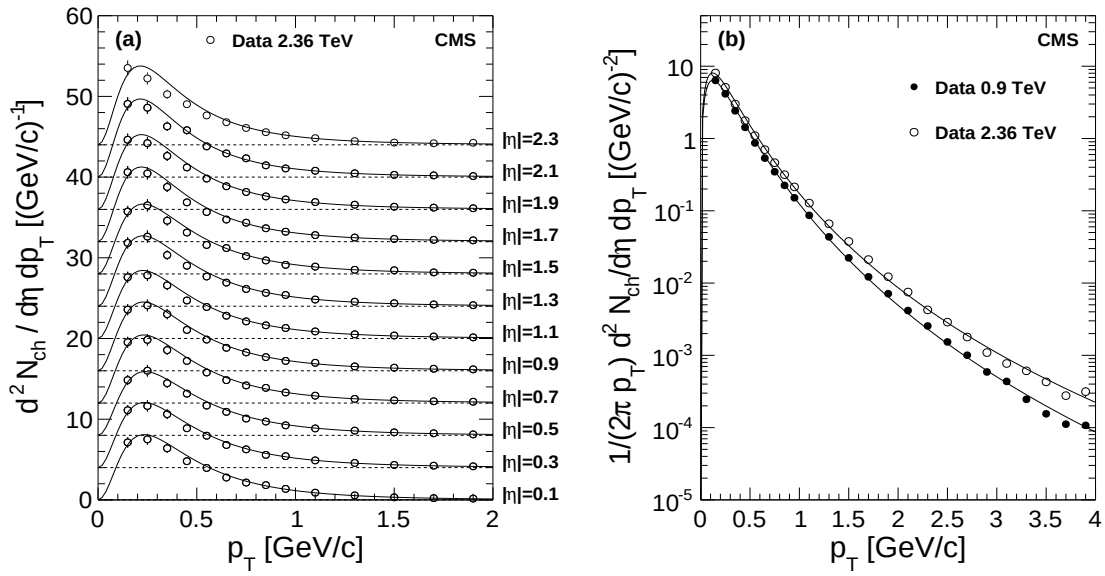

Figure 5: (a) Measured differential yield of charged hadrons in the range $|\eta| < 2.4$ in 0.2-unit-wide bins of $|\eta|$ for the 2.36 TeV data. The measured values with systematic uncertainties (symbols) and the fit functions (Eq. 1) are displayed. The values with increasing η are successively shifted by four units along the vertical axis. (b) Measured yield of charged hadrons for $|\eta| < 2.4$ with systematic uncertainties (symbols), fit with the empirical function (Eq. 1).

shown. The results from the three analysis methods are in agreement. The larger fraction of background hits in the data compared to simulation affects the cluster-counting method differently from the other two, which results in a small difference at high η, well accounted for by the systematic uncertainty of the measurement.

6 Discussion

The average transverse-momentum and pseudorapidity densities of charged hadrons derived from the measured data can be compared to results from earlier experiments as a function of the collision energy. The average transverse momentum of charged hadrons was obtained from the fits (Eq. 1) to the transverse-momentum spectrum (Fig. 5b). At low energies the energy dependence of $\langle p_{\mathrm{T}} \rangle$ can be described by a quadratic function of $\ln s$. The $\langle p_{\mathrm{T}} \rangle$ from this measurement, shown in Fig. 7a, follows the general trend. At 0.9 TeV it is similar to the results from $\mathrm{p\bar{p}}$ collisions at the same energy [22].

The $dN_{\mathrm{ch}}/d\eta$ distribution was calculated as the weighted average of the data from the three reconstruction methods, taking into account their systematic uncertainties, excluding the common ones, as listed in Table 3. The averaged result is shown in Fig. 6b and compared to measurements at the same accelerator (ALICE, pp [23]) and to previous measurements at the same energy but with different colliding particles (UA5, $\mathrm{p\bar{p}}$ [24]). The shaded error band on the CMS data indicates systematic uncertainties, while the error bars on the data from UA5 and ALICE display statistical uncertainties only. No significant difference is observed between the $dN_{\mathrm{ch}}/d\eta$ distributions measured in pp and $\mathrm{p\bar{p}}$ collisions at $\sqrt{s} = 0.9$ TeV.

The $dN_{\mathrm{ch}}/d\eta$ distribution is weakly η-dependent, with a slow increase towards higher η val-

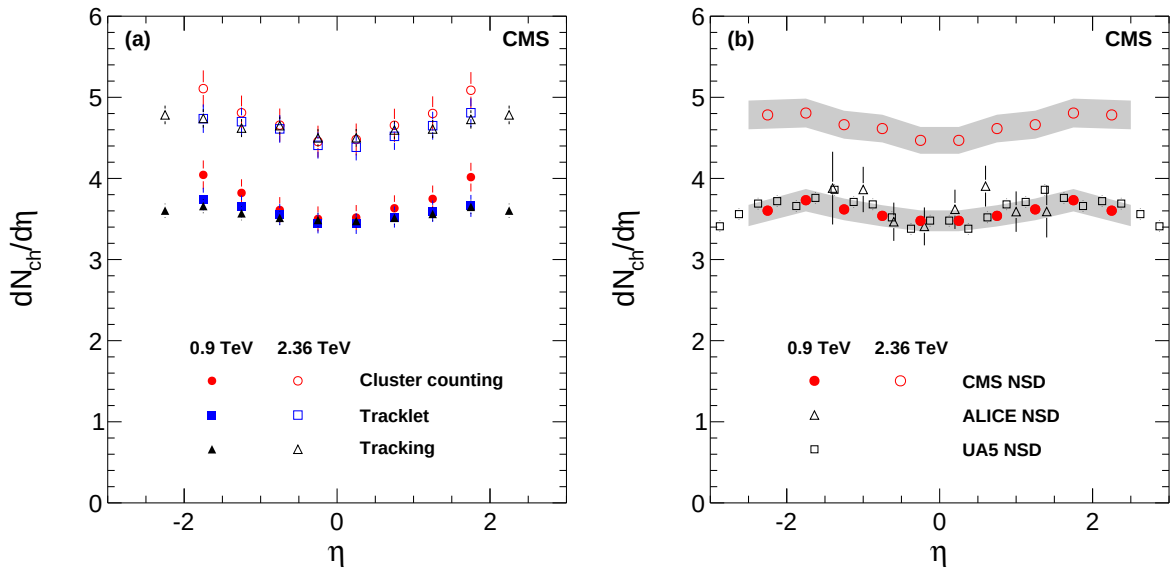

Figure 6: (a) Reconstructed $dN_{\mathrm{ch}}/d\eta$ distributions obtained from the cluster counting (dots with error bars), tracklet (squares) and tracking (triangles) methods, in pp collisions at 0.9 TeV (filled symbols) and 2.36 TeV (open symbols). The error bars include systematic uncertainties (as discussed in the text), excluding those common to all the methods. (b) Reconstructed $dN_{\mathrm{ch}}/d\eta$ distributions averaged over the cluster counting, tracklet and tracking methods (circles), compared to data from the UA5 [24] (open squares) and from the ALICE [23] (open triangles) experiments at 0.9 TeV, and the averaged result over the three methods at 2.36 TeV (open circles). The CMS and UA5 data points are symmetrized in η. The shaded band represents systematic uncertainties of this measurement, which are largely correlated point-to-point. The error bars on the UA5 and ALICE data points are statistical only.

ues, and an indication of a decrease at $|\eta| > 2$ for the 0.9 TeV data. At 2.36 TeV, the entire distribution is wider due to the increased collision energy hence the larger η range available for inclusive particle production. For $|\eta| < 0.5$, the corrected results average to $dN_{\mathrm{ch}}/d\eta = 3.48 \pm 0.02\,(\mathrm{stat.}) \pm 0.13\,(\mathrm{syst.})$ and $dN_{\mathrm{ch}}/d\eta = 4.47 \pm 0.04\,(\mathrm{stat.}) \pm 0.16\,(\mathrm{syst.})$ for NSD events at $\sqrt{s} = 0.9$ and 2.36 TeV. The increase of $(28.4 \pm 1.4 \pm 2.6)\%$ from 0.9 to 2.36 TeV is significantly larger than the 18.5% (14.5%) increase predicted by the PYTHIA (PHOJET) model tunes used in this analysis. The collision energy dependence of the measured $dN_{\mathrm{ch}}/d\eta|_{\eta\approx 0}$ is shown in Fig. 7b, which includes data from the NAL Bubble Chamber [25], the ISR [26], and UA1 [22], UA5 [24], CDF [27], STAR [28], PHOBOS [29] and ALICE [23]. The $dN_{\mathrm{ch}}/d\eta$ measurement reported here is consistent with the previously observed trend.

7 Summary

Inclusive measurements of charged-hadron densities, $dN_{\mathrm{ch}}/dp_{\mathrm{T}}$ and $dN_{\mathrm{ch}}/d\eta$, have been presented based on the first pp collisions recorded at $\sqrt{s} = 0.9$ and 2.36 TeV by the CMS experiment during LHC commissioning in December 2009. The numerical values of the data presented in this paper can be found in Ref. [30]. For NSD interactions, the average charged-hadron transverse momentum has been measured to be $0.46 \pm 0.01\,(\mathrm{stat.}) \pm 0.01\,(\mathrm{syst.})$ GeV/c at 0.9 TeV and $0.50 \pm 0.01\,(\mathrm{stat.}) \pm 0.01\,(\mathrm{syst.})$ GeV/c at 2.36 TeV. The three reconstruction methods

employed for the $dN_{\mathrm{ch}}/d\eta$ measurement have yielded consistent results, demonstrating the excellent performance and detailed understanding of the CMS tracker. The pseudorapidity density in the central region, $dN_{\mathrm{ch}}/d\eta|_{|\eta|<0.5}$, has been measured to be 3.48 ± 0.02 (stat.) $\pm$ 0.13 (syst.) at 0.9 TeV and 4.47 ± 0.04 (stat.) $\pm$ 0.16 (syst.) at 2.36 TeV. The results at 0.9 TeV have been found to be in agreement with previous measurements in $\mathrm{p\bar{p}}$ and pp collisions. With the new measurements at 2.36 TeV, which show a steeper-than-expected increase of charged-hadron multiplicity density with collision energy, the study of particle production in pp collisions has been extended into a new energy regime.

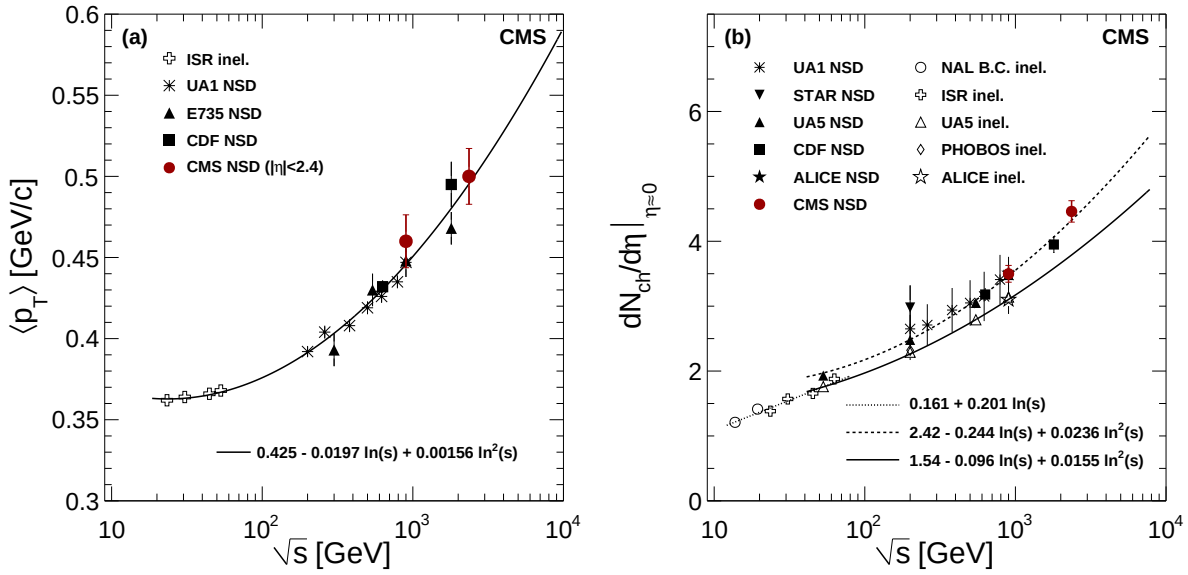

Figure 7: (a) Energy dependence of the average transverse momentum of charged hadrons. The CMS data points are evaluated for the range $|\eta| < 2.4$. Data of other experiments are taken from Refs. [22, 31–33]. The curve shows the fit to the data points of the form $\langle p_{\mathrm{T}} \rangle = 0.425 - 0.0197 \ln(s) + 0.00156 \ln^2(s)$ with $\langle p_{\mathrm{T}} \rangle$ in GeV/c and s in GeV^2. The error bars on the CMS data points include systematic uncertainties. (b) Charged-hadron pseudorapidity density in the central region as a function of centre-of-mass energy in pp and $\mathrm{p\bar{p}}$ collisions including lower energy data from Refs. [22–29], together with various empirical parameterizations fit to the data corresponding to the inelastic (solid and dotted curves with open symbols) and to the NSD (dashed curve with solid symbols) event selection. The error bars indicate systematic uncertainties, when available.

Acknowledgements

We congratulate and express our gratitude to our colleagues in the CERN accelerator departments for the excellent performance of the LHC. We thank the technical and administrative staff at CERN and other CMS Institutes, and acknowledge support from: FMSR (Austria); FNRS and FWO (Belgium); CNPq, CAPES, FAPERJ, and FAPESP (Brazil); MES (Bulgaria); CERN; CAS, MoST, and NSFC (China); COLCIENCIAS (Colombia); MSES (Croatia); RPF (Cyprus); Academy of Sciences and NICPB (Estonia); Academy of Finland, ME, and HIP (Finland); CEA and CNRS/IN2P3 (France); BMBF, DFG, and HGF (Germany); GSRT (Greece); OTKA and NKTH (Hungary); DAE and DST (India); IPM (Iran); SFI (Ireland); INFN (Italy); NRF (Korea); LAS (Lithuania); CINVESTAV, CONACYT, SEP, and UASLP-FAI

(Mexico); PAEC (Pakistan); SCSR (Poland); FCT (Portugal); JINR (Armenia, Belarus, Georgia, Ukraine, Uzbekistan); MST and MAE (Russia); MSTDS (Serbia); MICINN and CPAN (Spain); Swiss Funding Agencies (Switzerland); NSC (Taipei); TUBITAK and TAEK (Turkey); STFC (United Kingdom); DOE and NSF (USA). Individuals have received support from the Marie-Curie IEF program (European Union); the Leventis Foundation; the A. P. Sloan Foundation; and the Alexander von Humboldt Foundation.

References

[1] L. Evans, (ed.) and P. Bryant, (ed.), "LHC Machine", *JINST* **3** (2008) S08001. doi:10.1088/1748-0221/3/08/S08001.

[2] W. Kittel and E. A. De Wolf, "Soft Multihadron Dynamics". (World Scientific, Singapore, 2005).

[3] J. G. Rushbrooke and B. R. Webber, "High energy anti-particle-particle reaction differences and annihilations", *Phys. Rept.* **44** (1978) 1. doi:10.1016/0370-1573(78)90093-5.

[4] **CMS** Collaboration, "The CMS experiment at the CERN LHC", *JINST* **3** (2008) S08004. doi:10.1088/1748-0221/3/08/S08004.

[5] **CMS** Collaboration, "CMS Physics TDR: Volume I, Detector Performance and Software", *CERN-LHCC* **2006-001** (2006).

[6] **CMS** Collaboration, "Commissioning and Performance of the CMS Pixel Tracker with Cosmic Ray Muons", *submitted to JINST* (2009) arXiv:0911.5434.

[7] **CMS** Collaboration, "Alignment of the CMS Silicon Tracker during Commissioning with Cosmic Rays", *to appear in JINST* (2009) arXiv:0910.2505.

[8] A. J. Bell, "Design and Construction of the Beam Scintillation Counter for CMS", Master's thesis, University of Canterbury, Christchurch, New Zealand, 2008.

[9] T. Aumeyr, "Beam Phase and Intensity Monitoring for the Compact Muon Solenoid Experiment", Master's thesis, Vienna University of Technology, Austria, 2008.

[10] **Geant4** Collaboration, S. Agostinelli et al., "Geant4: a simulation toolkit", *Nucl. Instrum. and Methods* **A506** (2003) 250. doi:10.1016/S0168-9002(03)01368-8.

[11] T. Sjöstrand, S. Mrenna, and P. Skands, "PYTHIA 6.4 Physics and Manual; v6.420, tune D6T", *JHEP* **05** (2006) 026, arXiv:hep-ph/0603175.

[12] "Multiple Parton Interactions at the LHC. Proceedings, 1st Workshop, Perugia, Italy, October 27-31, 2008". DESY-PROC-2009-06.

[13] F. W. Bopp, R. Engel, and J. Ranft, "Rapidity gaps and the PHOJET Monte Carlo", arXiv:hep-ph/9803437.

[14] R. Engel, J. Ranft, and S. Roesler, "Hard diffraction in hadron-hadron interactions and in photoproduction", *Phys. Rev.* **D52** (1995) 1459, arXiv:hep-ph/9502319. doi:10.1103/PhysRevD.52.1459.

[15] F. Siklér, "Improved primary vertex finding for collider detectors", arXiv:0911.2767.

[16] **PHOBOS** Collaboration, B. B. Back et al., "Charged particle multiplicity near mid-rapidity in central Au + Au collisions at $\sqrt{s}$ = 56 and 130 AGeV", *Phys. Rev. Lett.* **85** (2000) 3100, arXiv:hep-ex/0007036. doi:10.1103/PhysRevLett.85.3100.

[17] S. Cucciarelli et al., "Track reconstruction, primary vertex finding and seed generation with the pixel detector", *CMS Note* **2006/026** (2006).

[18] T. Speer et al., "Track reconstruction in the CMS tracker", *Nucl. Instrum. and Methods* **A559** (2006) 143. doi:10.1016/j.nima.2005.11.207.

[19] **UA5** Collaboration, R. E. Ansorge et al., "Diffraction Dissociation at the CERN Pulsed p p-bar Collider at c.m. Energies of 900 and 200 GeV", *Z. Phys.* **C33** (1986) 175. doi:10.1007/BF01411134.

[20] C. Tsallis, "Possible generalization of Boltzmann-Gibbs statistics", *J. Stat. Phys.* **52** (1988) 479. doi:10.1007/BF01016429.

[21] G. Wilk and Z. Wlodarczyk, "Power laws in elementary and heavy-ion collisions: A Story of fluctuations and nonextensivity?", *Eur. Phys. J.* **A40** (2009) 299, arXiv:0810.2939. doi:10.1140/epja/i2009-10803-9.

[22] **UA1** Collaboration, C. Albajar et al., "A Study of the General Characteristics of Proton-Antiproton Collisions at 0.2 to 0.9 TeV", *Nucl. Phys.* **B335** (1990) 261. doi:10.1016/0550-3213(90)90493-W.

[23] **ALICE** Collaboration, K. Aamodt, "First proton–proton collisions at the LHC as observed with the ALICE detector: measurement of the charged-particle pseudorapidity density at $\sqrt{s}$ = 900 GeV", *Eur. Phys. J.* **C65** (2010) 111, arXiv:0911.5430. doi:10.1140/epjc/s10052-009-1227-4.

[24] **UA5** Collaboration, G. J. Alner et al., "Scaling of pseudorapidity distributions at c.m. energies up to 0.9 TeV", *Z. Phys.* **C33** (1986) 1. doi:10.1007/BF01410446.

[25] J. Whitmore, "Experimental Results on Strong Interactions in the NAL Hydrogen Bubble Chamber", *Phys. Rept.* **10** (1974) 273. doi:10.1016/0370-1573(74)90046-5.

[26] **Aachen-CERN-Heidelberg-Munich** Collaboration, W. Thome et al., "Charged Particle Multiplicity Distributions in p p Collisions at ISR Energies", *Nucl. Phys.* **B129** (1977) 365. doi:10.1016/0550-3213(77)90122-5.

[27] **CDF** Collaboration, F. Abe et al., "Pseudorapidity distributions of charged particles produced in $p\bar{p}$ interactions at $\sqrt{s} = 630$ GeV and 1800 GeV", *Phys. Rev.* **D41** (1990) 2330. doi:10.1103/PhysRevD.41.2330.

[28] **STAR** Collaboration, B. I. Abelev et al., "Systematic measurements of identified particle spectra in p+p, d+Au and Au+Au collisions at the STAR detector", *Phys. Rev.* **C79** (2009) 034909, arXiv:0808.2041. doi:10.1103/PhysRevC.79.034909.

[29] **PHOBOS** Collaboration, R. Nouicer et al., "Pseudorapidity distributions of charged particles in d+Au and p+p collisions at $\sqrt{s_{\mathrm{NN}}} = 200$ GeV", *J. Phys.* **G30** (2004) S1133, arXiv:nucl-ex/0403033. doi:10.1088/0954-3899/30/8/075.

[30] **CMS** Collaboration, "Numerical values of the data presented in this paper", 2010.

[31] A. M. Rossi et al., "Experimental Study of the Energy Dependence in Proton Proton Inclusive Reactions", *Nucl. Phys.* **B84** (1975) 269. doi:10.1016/0550-3213(75)90307-7.

[32] **E735** Collaboration, T. Alexopoulos et al., "Multiplicity dependence of the transverse momentum spectrum for centrally produced hadrons in antiproton - proton collisions at $\sqrt{s}$ = 1.8 TeV", *Phys. Rev. Lett.* **60** (1988) 1622. doi:10.1103/PhysRevLett.60.1622.

[33] **CDF** Collaboration, F. Abe et al., "Transverse momentum distributions of charged particles produced in $\bar{p}p$ interactions at $\sqrt{s} = 630$ GeV and 1800 GeV", *Phys. Rev. Lett.* **61** (1988) 1819. doi:10.1103/PhysRevLett.61.1819.

A The CMS Collaboration

Yerevan Physics Institute, Yerevan, Armenia
V. Khachatryan, A.M. Sirunyan, A. Tumasyan

Institut für Hochenergiephysik der OeAW, Wien, Austria
W. Adam, T. Bergauer, M. Dragicevic, J. Erö, M. Friedl, R. Frühwirth, V.M. Ghete, J. Hammer[1], S. Hänsel, M. Hoch, N. Hörmann, J. Hrubec, M. Jeitler, G. Kasieczka, M. Krammer, D. Liko, I. Mikulec, M. Pernicka, H. Rohringer, R. Schöfbeck, J. Strauss, A. Taurok, F. Teischinger, W. Waltenberger, G. Walzel, E. Widl, C.-E. Wulz

National Centre for Particle and High Energy Physics, Minsk, Belarus
V. Mossolov, N. Shumeiko, J. Suarez Gonzalez

Universiteit Antwerpen, Antwerpen, Belgium
L. Benucci, E.A. De Wolf, M. Hashemi, X. Janssen, T. Maes, L. Mucibello, S. Ochesanu, R. Rougny, M. Selvaggi, H. Van Haevermaet, P. Van Mechelen, N. Van Remortel

Vrije Universiteit Brussel, Brussel, Belgium
V. Adler, S. Beauceron, J. D'Hondt, O. Devroede, A. Kalogeropoulos, J. Maes, M.U. Mozer, S. Tavernier, W. Van Doninck, P. Van Mulders, I. Villella

Université Libre de Bruxelles, Bruxelles, Belgium
E.C. Chabert, O. Charaf, B. Clerbaux, G. De Lentdecker, V. Dero, A.P.R. Gay, G.H. Hammad, P.E. Marage, C. Vander Velde, P. Vanlaer, J. Wickens

Ghent University, Ghent, Belgium
M. Grunewald, B. Klein, A. Marinov, D. Ryckbosch, F. Thyssen, M. Tytgat, L. Vanelderen, P. Verwilligen, S. Walsh

Université Catholique de Louvain, Louvain-la-Neuve, Belgium
S. Basegmez, G. Bruno, J. Caudron, E. Cortina Gil, J. De Favereau De Jeneret, C. Delaere, P. Demin, D. Favart, A. Giammanco, G. Grégoire, J. Hollar, V. Lemaitre, F. Maltoni, O. Militaru, S. Ovyn, K. Piotrzkowski[1], L. Quertenmont, N. Schul

Université de Mons, Mons, Belgium
N. Beliy, T. Caebergs, E. Daubie, P. Herquet

Centro Brasileiro de Pesquisas Fisicas, Rio de Janeiro, Brazil
G.A. Alves, M.E. Pol, M.H.G. Souza

Universidade do Estado do Rio de Janeiro, Rio de Janeiro, Brazil
W. Carvalho, E.M. Da Costa, D. De Jesus Damiao, C. De Oliveira Martins, S. Fonseca De Souza, L. Mundim, V. Oguri, A. Santoro, S.M. Silva Do Amaral, A. Sznajder, F. Torres Da Silva De Araujo

Instituto de Fisica Teorica, Universidade Estadual Paulista, Sao Paulo, Brazil
F.A. Dias, M.A.F. Dias, T.R. Fernandez Perez Tomei, E. M. Gregores[2], F. Marinho, S.F. Novaes, Sandra S. Padula

Institute for Nuclear Research and Nuclear Energy, Sofia, Bulgaria
J. Damgov, N. Darmenov[1], L. Dimitrov, V. Genchev[1], P. Iaydjiev, S. Piperov, S. Stoykova, G. Sultanov, R. Trayanov, I. Vankov

University of Sofia, Sofia, Bulgaria
R. Hadjiiska, V. Kozhuharov, L. Litov, M. Mateev, B. Pavlov, P. Petkov

Institute of High Energy Physics, Beijing, China
G.M. Chen, H.S. Chen, C.H. Jiang, D. Liang, S. Liang, X. Meng, J. Tao, J. Wang, J. Wang, X. Wang, Z. Wang, J. Zang, Z. Zhang

State Key Lab. of Nucl. Phys. and Tech., Peking University, Beijing, China
Y. Ban, S. Guo, Z. Hu, Y. Mao, S.J. Qian, H. Teng, B. Zhu

Universidad de Los Andes, Bogota, Colombia
C.A. Carrillo Montoya, B. Gomez Moreno, A.A. Ocampo Rios, J.C. Sanabria

Technical University of Split, Split, Croatia
N. Godinovic, K. Lelas, R. Plestina, D. Polic, I. Puljak

University of Split, Split, Croatia
Z. Antunovic, M. Dzelalija

Institute Rudjer Boskovic, Zagreb, Croatia
V. Brigljevic, S. Duric, K. Kadija, S. Morovic

University of Cyprus, Nicosia, Cyprus
A. Attikis, R. Fereos, M. Galanti, J. Mousa, A. Papadakis, F. Ptochos, P.A. Razis, D. Tsiakkouri, Z. Zinonos

National Institute of Chemical Physics and Biophysics, Tallinn, Estonia
A. Hektor, M. Kadastik, K. Kannike, M. Müntel, M. Raidal, L. Rebane

Department of Physics, University of Helsinki, Helsinki, Finland
P. Eerola

Helsinki Institute of Physics, Helsinki, Finland
S. Czellar, J. Härkönen, A. Heikkinen, V. Karimäki, R. Kinnunen, J. Klem, M.J. Kortelainen, T. Lampén, K. Lassila-Perini, S. Lehti, T. Lindén, P. Luukka, T. Mäenpää, E. Tuominen, J. Tuominiemi, E. Tuovinen, D. Ungaro, L. Wendland

Lappeenranta University of Technology, Lappeenranta, Finland
K. Banzuzi, A. Korpela, T. Tuuva

Laboratoire d'Annecy-le-Vieux de Physique des Particules, IN2P3-CNRS, Annecy-le-Vieux, France
D. Sillou

DSM/IRFU, CEA/Saclay, Gif-sur-Yvette, France
M. Besancon, M. Dejardin, D. Denegri, J. Descamps, B. Fabbro, J.L. Faure, F. Ferri, S. Ganjour, F.X. Gentit, A. Givernaud, P. Gras, G. Hamel de Monchenault, P. Jarry, E. Locci, J. Malcles, M. Marionneau, L. Millischer, J. Rander, A. Rosowsky, D. Rousseau, M. Titov, P. Verrecchia

Laboratoire Leprince-Ringuet, Ecole Polytechnique, IN2P3-CNRS, Palaiseau, France
S. Baffioni, L. Bianchini, C. Broutin, P. Busson, C. Charlot, L. Dobrzynski, S. Elgammal, R. Granier de Cassagnac, M. Haguenauer, P. Miné, P. Paganini, Y. Sirois, C. Thiebaux, A. Zabi

Institut Pluridisciplinaire Hubert Curien, Université de Strasbourg, Université de Haute Alsace Mulhouse, CNRS/IN2P3, Strasbourg, France
J.-L. Agram[3], A. Besson, D. Bloch, D. Bodin, J.-M. Brom, M. Cardaci, E. Conte[3], F. Drouhin[3], C. Ferro, J.-C. Fontaine[3], D. Gelé, U. Goerlach, S. Greder, P. Juillot, A.-C. Le Bihan, Y. Mikami, I. Ripp-Baudot, J. Speck, P. Van Hove

Université de Lyon, Université Claude Bernard Lyon 1, CNRS-IN2P3, Institut de Physique Nucléaire de Lyon, Villeurbanne, France
C. Baty, M. Bedjidian, O. Bondu, G. Boudoul, D. Boumediene, H. Brun, N. Chanon, R. Chierici, D. Contardo, P. Depasse, H. El Mamouni, F. Fassi[4], J. Fay, S. Gascon, B. Ille, T. Kurca, T. Le Grand, M. Lethuillier, L. Mirabito, S. Perries, S. Tosi, Y. Tschudi, P. Verdier, H. Xiao

E. Andronikashvili Institute of Physics, Academy of Science, Tbilisi, Georgia
V. Roinishvili

RWTH Aachen University, I. Physikalisches Institut, Aachen, Germany
G. Anagnostou, M. Edelhoff, L. Feld, N. Heracleous, O. Hindrichs, R. Jussen, K. Klein, J. Merz, N. Mohr, A. Ostapchuk, D. Pandoulas, A. Perieanu, F. Raupach, J. Sammet, S. Schael, D. Sprenger, H. Weber, M. Weber, B. Wittmer

RWTH Aachen University, III. Physikalisches Institut A, Aachen, Germany
O. Actis, W. Bender, P. Biallass, M. Erdmann, J. Frangenheim, T. Hebbeker, A. Hinzmann, K. Hoepfner, C. Hof, M. Kirsch, T. Klimkovich, P. Kreuzer[1], D. Lanske[†], M. Merschmeyer, A. Meyer, H. Pieta, H. Reithler, S.A. Schmitz, M. Sowa, J. Steggemann, D. Teyssier, C. Zeidler

RWTH Aachen University, III. Physikalisches Institut B, Aachen, Germany
M. Bontenackels, M. Davids, M. Duda, G. Flügge, H. Geenen, M. Giffels, W. Haj Ahmad, D. Heydhausen, T. Kress, Y. Kuessel, A. Linn, A. Nowack, L. Perchalla, O. Pooth, P. Sauerland, A. Stahl, M. Thomas, D. Tornier, M.H. Zoeller

Deutsches Elektronen-Synchrotron, Hamburg, Germany
M. Aldaya Martin, U. Behrens, K. Borras, A. Campbell, E. Castro, D. Dammann, G. Eckerlin, A. Flossdorf, G. Flucke, A. Geiser, J. Hauk, H. Jung, M. Kasemann, I. Katkov, C. Kleinwort, H. Kluge, A. Knutsson, E. Kuznetsova, W. Lange, W. Lohmann, R. Mankel[1], M. Marienfeld, A.B. Meyer, J. Mnich, J. Olzem, A. Parenti, R. Schmidt, T. Schoerner-Sadenius, N. Sen, M. Stein, D. Volyanskyy, C. Wissing

University of Hamburg, Hamburg, Germany
C. Autermann, J. Draeger, D. Eckstein, H. Enderle, U. Gebbert, K. Kaschube, G. Kaussen, R. Klanner, B. Mura, S. Naumann-Emme, F. Nowak, C. Sander, P. Schleper, M. Schröder, T. Schum, H. Stadie, G. Steinbrück, J. Thomsen, R. Wolf

Institut für Experimentelle Kernphysik, Karlsruhe, Germany
J. Bauer, P. Blüm, V. Buege, A. Cakir, T. Chwalek, D. Daeuwel, W. De Boer, A. Dierlamm, G. Dirkes, M. Feindt, M. Frey, J. Gruschke, C. Hackstein, F. Hartmann, M. Heinrich, K.H. Hoffmann, S. Honc, T. Kuhr, D. Martschei, S. Mueller, Th. Müller, M. Niegel, O. Oberst, A. Oehler, J. Ott, T. Peiffer, D. Piparo, G. Quast, K. Rabbertz, M. Renz, A. Sabellek, C. Saout[1], A. Scheurer, P. Schieferdecker, F.-P. Schilling, G. Schott, H.J. Simonis, F.M. Stober, J. Wagner-Kuhr, M. Zeise, V. Zhukov[5], E.B. Ziebarth

Institute of Nuclear Physics "Demokritos", Aghia Paraskevi, Greece
G. Daskalakis, T. Geralis, K. Karafasoulis, A. Kyriakis, D. Loukas, A. Markou, C. Markou, C. Mavrommatis, E. Petrakou, A. Zachariadou

University of Athens, Athens, Greece
A. Agapitos, L. Gouskos, P. Katsas, A. Panagiotou, K. Saganis, E. Xaxiris

University of Ioánnina, Ioánnina, Greece
I. Evangelou, P. Kokkas, N. Manthos, I. Papadopoulos, F.A. Triantis

KFKI Research Institute for Particle and Nuclear Physics, Budapest, Hungary
A. Aranyi, G. Bencze, L. Boldizsar, G. Debreczeni, C. Hajdu[1], D. Horvath[6], A. Kapusi, K. Krajczar, A. Laszlo, F. Sikler, G. Vesztergombi

Institute of Nuclear Research ATOMKI, Debrecen, Hungary
N. Beni, J. Molnar, J. Palinkas, Z. Szillasi[1], V. Veszpremi

University of Debrecen, Debrecen, Hungary
P. Raics, Z.L. Trocsanyi, B. Ujvari

Panjab University, Chandigarh, India
S. Bansal, S.B. Beri, V. Bhatnagar, M. Jindal, M. Kaur, J.M. Kohli, M.Z. Mehta, N. Nishu, L.K. Saini, A. Sharma, R. Sharma, A.P. Singh, J.B. Singh, S.P. Singh

University of Delhi, Delhi, India
S. Ahuja, S. Bhattacharya[7], S. Chauhan, B.C. Choudhary, P. Gupta, S. Jain, S. Jain, A. Kumar, K. Ranjan, R.K. Shivpuri

Bhabha Atomic Research Centre, Mumbai, India
R.K. Choudhury, D. Dutta, S. Kailas, S.K. Kataria, A.K. Mohanty, L.M. Pant, P. Shukla, P. Suggisetti

Tata Institute of Fundamental Research - EHEP, Mumbai, India
T. Aziz, M. Guchait[8], A. Gurtu, M. Maity[9], D. Majumder, G. Majumder, K. Mazumdar, A. Nayak, A. Saha, K. Sudhakar, N. Wickramage

Tata Institute of Fundamental Research - HECR, Mumbai, India
S. Banerjee, S. Dugad, N.K. Mondal

Institute for Studies in Theoretical Physics & Mathematics (IPM), Tehran, Iran
H. Arfaei, H. Bakhshiansohi, A. Fahim, A. Jafari, M. Mohammadi Najafabadi, A. Moshaii, S. Paktinat Mehdiabadi, M. Zeinali

University College Dublin, Dublin, Ireland
M. Felcini

INFN Sezione di Bari [a], Università di Bari [b], Politecnico di Bari [c], Bari, Italy
M. Abbrescia[a,b], L. Barbone[a], A. Colaleo[a], D. Creanza[a,c], N. De Filippis[a], M. De Palma[a,b], A. Dimitrov, F. Fedele[a], L. Fiore[a], G. Iaselli[a,c], L. Lusito[a,b,1], G. Maggi[a,c], M. Maggi[a], N. Manna[a,b], B. Marangelli[a,b], S. My[a,c], S. Nuzzo[a,b], G.A. Pierro[a], G. Polese, A. Pompili[a,b], G. Pugliese[a,c], F. Romano[a,c], G. Roselli[a,b], G. Selvaggi[a,b], L. Silvestris[a], S. Tupputi[a,b], G. Zito[a]

INFN Sezione di Bologna [a], Università di Bologna [b], Bologna, Italy
G. Abbiendi[a], D. Bonacorsi[a], S. Braibant-Giacomelli[a,b], P. Capiluppi[a,b], F.R. Cavallo[a], G. Codispoti[a,b], M. Cuffiani[a,b], G.M. Dallavalle[a,1], F. Fabbri[a], A. Fanfani[a,b], D. Fasanella[a], P. Giacomelli[a], M. Giunta[a,1], C. Grandi[a], S. Marcellini[a], G. Masetti[a,b], A. Montanari[a], F.L. Navarria[a,b], F. Odorici[a], A. Perrotta[a], A.M. Rossi[a,b], T. Rovelli[a,b], G. Siroli[a,b], R. Travaglini[a,b]

INFN Sezione di Catania [a], Università di Catania [b], Catania, Italy
S. Albergo[a,b], M. Chiorboli[a,b], S. Costa[a,b], R. Potenza[a,b], A. Tricomi[a,b], C. Tuve[a]

INFN Sezione di Firenze [a], Università di Firenze [b], Firenze, Italy
G. Barbagli[a], G. Broccolo[a,b], V. Ciulli[a,b], C. Civinini[a], R. D'Alessandro[a,b], E. Focardi[a,b], S. Frosali[a,b], E. Gallo[a], C. Genta[a,b], G. Landi[a,b], P. Lenzi[a,b,1], M. Meschini[a], S. Paoletti[a], G. Sguazzoni[a], A. Tropiano[a]

INFN Laboratori Nazionali di Frascati, Frascati, Italy
S. Bianco, S. Colafranceschi[10], F. Fabbri, D. Piccolo

INFN Sezione di Genova, Genova, Italy
P. Fabbricatore, R. Musenich

INFN Sezione di Milano-Biccoca [a], Università di Milano-Bicocca [b], Milano, Italy
A. Benaglia[a], G.B. Cerati[a,b,1], F. De Guio[a], A. Ghezzi[a,1], P. Govoni[a,b], M. Malberti[a,b,1], S. Malvezzi[a], A. Martelli[a], D. Menasce[a], V. Miccio[a,b], L. Moroni[a], P. Negri[a,b], M. Paganoni[a,b], D. Pedrini[a], A. Pullia[a,b], S. Ragazzi[a,b], N. Redaelli[a], S. Sala[a], R. Salerno[a,b], T. Tabarelli de Fatis[a,b], V. Tancini[a,b], S. Taroni[a,b]

INFN Sezione di Napoli [a], Università di Napoli "Federico II" [b], Napoli, Italy
A. Cimmino[a,b,1], M. De Gruttola[a,b,1], F. Fabozzi[a,11], A.O.M. Iorio[a], L. Lista[a], P. Noli[a,b], P. Paolucci[a]

INFN Sezione di Padova [a], Università di Padova [b], Università di Trento (Trento) [c], Padova, Italy
P. Azzi[a], N. Bacchetta[a], P. Bellan[a,b,1], M. Biasotto[a,12], R. Carlin[a,b], P. Checchia[a], M. De Mattia[a,b], T. Dorigo[a], F. Fanzago[a], F. Gasparini[a,b], P. Giubilato[a,b], F. Gonella[a], A. Gresele[a,c], M. Gulmini[a,12], S. Lacaprara[a,12], I. Lazzizzera[a,c], G. Maron[a,12], S. Mattiazzo[a,b], A.T. Meneguzzo[a,b], M. Passaseo[a], M. Pegoraro[a], N. Pozzobon[a,b], P. Ronchese[a,b], E. Torassa[a], M. Tosi[a,b], S. Vanini[a,b], S. Ventura[a], P. Zotto[a,b]

INFN Sezione di Pavia [a], Università di Pavia [b], Pavia, Italy
P. Baesso[a,b], U. Berzano[a], D. Pagano[a,b], S.P. Ratti[a,b], C. Riccardi[a,b], P. Torre[a,b], P. Vitulo[a,b], C. Viviani[a,b]

INFN Sezione di Perugia [a], Università di Perugia [b], Perugia, Italy
M. Biasini[a,b], G.M. Bilei[a], B. Caponeri[a,b], L. Fanò[a], P. Lariccia[a,b], A. Lucaroni[a,b], G. Mantovani[a,b], A. Nappi[a,b], A. Santocchia[a,b], L. Servoli[a], R. Volpe[a,b,1]

INFN Sezione di Pisa [a], Università di Pisa [b], Scuola Normale Superiore di Pisa [c], Pisa, Italy
P. Azzurri[a,c], G. Bagliesi[a], J. Bernardini[a,b], T. Boccali[a], A. Bocci[a,c], R. Castaldi[a], R. Dell'Orso[a], S. Dutta[a], F. Fiori[a,b], L. Foà[a,c], S. Gennai[a,c], A. Giassi[a], A. Kraan[a], F. Ligabue[a,c], T. Lomtadze[a], L. Martini[a], A. Messineo[a,b], F. Palla[a], F. Palmonari[a], S. Sarkar[a], G. Segneri[a], A.T. Serban[a], P. Spagnolo[a,1], R. Tenchini[a,1], G. Tonelli[a,b,1], A. Venturi[a], P.G. Verdini[a]

INFN Sezione di Roma [a], Università di Roma "La Sapienza" [b], Roma, Italy
L. Barone[a,b], F. Cavallari[a,1], D. Del Re[a,b], E. Di Marco[a,b], M. Diemoz[a], D. Franci[a,b], M. Grassi[a], E. Longo[a,b], G. Organtini[a,b], A. Palma[a,b], F. Pandolfi[a,b], R. Paramatti[a,1], S. Rahatlou[a,b], C. Rovelli[a]

INFN Sezione di Torino [a], Università di Torino [b], Università del Piemonte Orientale (Novara) [c], Torino, Italy
N. Amapane[a,b], R. Arcidiacono[a,b], S. Argiro[a,b], M. Arneodo[a,c], C. Biino[a], M.A. Borgia[a,b], C. Botta[a,b], N. Cartiglia[a], R. Castello[a,b], M. Costa[a,b], G. Dellacasa[a], N. Demaria[a], A. Graziano[a,b], C. Mariotti[a], M. Marone[a,b], S. Maselli[a], E. Migliore[a,b], G. Mila[a,b], V. Monaco[a,b], M. Musich[a,b], M.M. Obertino[a,c], N. Pastrone[a], A. Romero[a,b], M. Ruspa[a,c], R. Sacchi[a,b], A. Solano[a,b], A. Staiano[a], D. Trocino[a,b], A. Vilela Pereira[a,b,1]

INFN Sezione di Trieste [a], Università di Trieste [b], Trieste, Italy
F. Ambroglini[a,b], S. Belforte[a], F. Cossutti[a], G. Della Ricca[a,b], B. Gobbo[a], A. Penzo[a]

Kyungpook National University, Daegu, Korea
S. Chang, J. Chung, D.H. Kim, G.N. Kim, D.J. Kong, H. Park, D.C. Son

Chonnam National University, Kwangju, Korea
Zero Kim, S. Song

Konkuk University, Seoul, Korea
S.Y. Jung

Korea University, Seoul, Korea
B. Hong, H. Kim, J.H. Kim, K.S. Lee, D.H. Moon, S.K. Park, H.B. Rhee, K.S. Sim

Seoul National University, Seoul, Korea
J. Kim

University of Seoul, Seoul, Korea
M. Choi, I.C. Park

Sungkyunkwan University, Suwon, Korea
S. Choi, Y. Choi, Y.K. Choi, J. Goh, Y. Jo, J. Kwon, J. Lee, S. Lee

Vilnius University, Vilnius, Lithuania
M. Janulis, D. Martisiute, P. Petrov, T. Sabonis

Centro de Investigacion y de Estudios Avanzados del IPN, Mexico City, Mexico
H. Castilla Valdez[1], A. Sánchez Hernández

Universidad Iberoamericana, Mexico City, Mexico
S. Carrillo Moreno

Benemerita Universidad Autonoma de Puebla, Puebla, Mexico
H.A. Salazar Ibarguen

Universidad Autónoma de San Luis Potosí, San Luis Potosí, Mexico
E. Casimiro Linares, A. Morelos Pineda

University of Auckland, Auckland, New Zealand
P. Allfrey, D. Krofcheck

University of Canterbury, Christchurch, New Zealand
T. Aumeyr, P.H. Butler, T. Signal, J.C. Williams

National Centre for Physics, Quaid-I-Azam University, Islamabad, Pakistan
M. Ahmad, I. Ahmed, M.I. Asghar, H.R. Hoorani, W.A. Khan, T. Khurshid, S. Qazi

Institute of Experimental Physics, Warsaw, Poland
M. Cwiok, W. Dominik, K. Doroba, M. Konecki, J. Krolikowski

Soltan Institute for Nuclear Studies, Warsaw, Poland
T. Frueboes, R. Gokieli, M. Górski, M. Kazana, K. Nawrocki, M. Szleper, G. Wrochna, P. Zalewski

Laboratório de Instrumentação e Física Experimental de Partículas, Lisboa, Portugal
N. Almeida, P. Bargassa, A. David, P. Faccioli, P.G. Ferreira Parracho, M. Gallinaro, P. Musella, P.Q. Ribeiro, J. Seixas, P. Silva, J. Varela[1], H.K. Wöhri

Joint Institute for Nuclear Research, Dubna, Russia
I. Altsybeev, I. Belotelov, P. Bunin, M. Finger, M. Finger Jr., I. Golutvin, A. Kamenev,

V. Karjavin, G. Kozlov, A. Lanev, P. Moisenz, V. Palichik, V. Perelygin, S. Shmatov, V. Smirnov, A. Vishnevskiy, A. Volodko, A. Zarubin

Petersburg Nuclear Physics Institute, Gatchina (St Petersburg), Russia
Y. Ivanov, V. Kim, P. Levchenko, G. Obrant, Y. Shcheglov, A. Shchetkovskiy, I. Smirnov, V. Sulimov, S. Vavilov, A. Vorobyev

Institute for Nuclear Research, Moscow, Russia
Yu. Andreev, S. Gninenko, N. Golubev, A. Karneyeu, M. Kirsanov, N. Krasnikov, V. Matveev, A. Pashenkov, A. Toropin, S. Troitsky

Institute for Theoretical and Experimental Physics, Moscow, Russia
V. Epshteyn, V. Gavrilov, N. Ilina, V. Kaftanov†, M. Kossov[1], A. Krokhotin, S. Kuleshov, A. Oulianov, G. Safronov, S. Semenov, I. Shreyber, V. Stolin, E. Vlasov, A. Zhokin

Moscow State University, Moscow, Russia
E. Boos, M. Dubinin[13], L. Dudko, A. Ershov, A. Gribushin, O. Kodolova, I. Lokhtin, S. Petrushanko, L. Sarycheva, V. Savrin, I. Vardanyan

P.N. Lebedev Physical Institute, Moscow, Russia
I. Dremin, M. Kirakosyan, N. Konovalova, S.V. Rusakov, A. Vinogradov

State Research Center of Russian Federation, Institute for High Energy Physics, Protvino, Russia
I. Azhgirey, S. Bitioukov, K. Datsko, V. Kachanov, D. Konstantinov, V. Krychkine, V. Petrov, R. Ryutin, S. Slabospitsky, A. Sobol, A. Sytine, L. Tourtchanovitch, S. Troshin, N. Tyurin, A. Uzunian, A. Volkov

Vinca Institute of Nuclear Sciences, Belgrade, Serbia
P. Adzic, M. Djordjevic, D. Maletic, J. Puzovic[14]

Centro de Investigaciones Energéticas Medioambientales y Tecnológicas (CIEMAT), Madrid, Spain
M. Aguilar-Benitez, J. Alcaraz Maestre, P. Arce, C. Battilana, E. Calvo, M. Cepeda, M. Cerrada, M. Chamizo Llatas, N. Colino, B. De La Cruz, C. Diez Pardos, C. Fernandez Bedoya, J.P. Fernández Ramos, A. Ferrando, J. Flix, M.C. Fouz, P. Garcia-Abia, O. Gonzalez Lopez, S. Goy Lopez, J.M. Hernandez, M.I. Josa, G. Merino, J. Puerta Pelayo, L. Romero, J. Santaolalla, C. Willmott

Universidad Autónoma de Madrid, Madrid, Spain
C. Albajar, J.F. de Trocóniz

Universidad de Oviedo, Oviedo, Spain
J. Cuevas, J. Fernandez Menendez, I. Gonzalez Caballero, L. Lloret Iglesias, J.M. Vizan Garcia

Instituto de Física de Cantabria (IFCA), CSIC-Universidad de Cantabria, Santander, Spain
I.J. Cabrillo, A. Calderon, S.H. Chuang, I. Diaz Merino, C. Diez Gonzalez, J. Duarte Campderros, M. Fernandez, G. Gomez, J. Gonzalez Sanchez, R. Gonzalez Suarez, C. Jorda, P. Lobelle Pardo, A. Lopez Virto, J. Marco, R. Marco, C. Martinez Rivero, P. Martinez Ruiz del Arbol, F. Matorras, T. Rodrigo, A. Ruiz Jimeno, L. Scodellaro, M. Sobron Sanudo, I. Vila, R. Vilar Cortabitarte

CERN, European Organization for Nuclear Research, Geneva, Switzerland
D. Abbaneo, E. Auffray, P. Baillon, A.H. Ball, D. Barney, F. Beaudette[15], B. Beccati, A.J. Bell[16], R. Bellan, D. Benedetti, C. Bernet, W. Bialas, P. Bloch, S. Bolognesi, M. Bona, H. Breuker,

K. Bunkowski, T. Camporesi, E. Cano, A. Cattai, G. Cerminara, T. Christiansen, J.A. Coarasa Perez, R. Covarelli, B. Curé, T. Dahms, A. De Roeck, A. Elliott-Peisert, W. Funk, A. Gaddi, H. Gerwig, D. Gigi, K. Gill, D. Giordano, F. Glege, S. Gowdy, L. Guiducci, J. Gutleber, C. Hartl, J. Harvey, B. Hegner, C. Henderson, H.F. Hoffmann, A. Honma, M. Huhtinen, V. Innocente, P. Janot, P. Lecoq, C. Leonidopoulos, C. Lourenço, A. Macpherson, T. Mäki, L. Malgeri, M. Mannelli, L. Masetti, F. Meijers, P. Meridiani, S. Mersi, E. Meschi, R. Moser, M. Mulders, M. Noy, T. Orimoto, L. Orsini, E. Perez, A. Petrilli, A. Pfeiffer, M. Pierini, M. Pimiä, A. Racz, G. Rolandi[17], M. Rovere, V. Ryjov, H. Sakulin, C. Schäfer, W.D. Schlatter, C. Schwick, I. Segoni, A. Sharma, P. Siegrist, M. Simon, P. Sphicas[18], D. Spiga, M. Spiropulu[13], F. Stöckli, P. Traczyk, P. Tropea, A. Tsirou, G.I. Veres[19], P. Vichoudis, M. Voutilainen, W.D. Zeuner

Paul Scherrer Institut, Villigen, Switzerland
W. Bertl, K. Deiters, W. Erdmann, K. Gabathuler, R. Horisberger, Q. Ingram, H.C. Kaestli, S. König, D. Kotlinski, U. Langenegger, F. Meier, D. Renker, T. Rohe, J. Sibille[20], A. Starodumov[21]

Institute for Particle Physics, ETH Zurich, Zurich, Switzerland
L. Caminada[22], M.C. Casella, Z. Chen, S. Cittolin, S. Dambach[22], G. Dissertori, M. Dittmar, C. Eggel[22], J. Eugster, K. Freudenreich, C. Grab, A. Hervé, W. Hintz, P. Lecomte, W. Lustermann, C. Marchica[22], P. Milenovic[23], F. Moortgat, A. Nardulli, F. Nessi-Tedaldi, L. Pape, F. Pauss, T. Punz, A. Rizzi, F.J. Ronga, L. Sala, A.K. Sanchez, M.-C. Sawley, D. Schinzel, V. Sordini, B. Stieger, L. Tauscher†, A. Thea, K. Theofilatos, D. Treille, P. Trüb[22], M. Weber, L. Wehrli, J. Weng

Universität Zürich, Zurich, Switzerland
C. Amsler, V. Chiochia, S. De Visscher, M. Ivova Rikova, C. Regenfus, P. Robmann, T. Rommerskirchen, A. Schmidt, H. Snoek, D. Tsirigkas, L. Wilke

National Central University, Chung-Li, Taiwan
Y.H. Chang, E.A. Chen, W.T. Chen, A. Go, C.M. Kuo, S.W. Li, W. Lin, M.H. Liu, J.H. Wu

National Taiwan University (NTU), Taipei, Taiwan
P. Bartalini, P. Chang, Y.H. Chang, Y. Chao, K.F. Chen, W.-S. Hou, Y. Hsiung, Y.J. Lei, S.W. Lin, R.-S. Lu, J.G. Shiu, Y.M. Tzeng, K. Ueno, C.C. Wang, M. Wang

Cukurova University, Adana, Turkey
A. Adiguzel, A. Ayhan, M.N. Bakirci, S. Cerci, Z. Demir, C. Dozen, I. Dumanoglu, E. Eskut, S. Girgis, E. Gurpinar, T. Karaman, A. Kayis Topaksu, G. Önengüt, K. Ozdemir, S. Ozturk, A. Polatöz, O. Sahin, O. Sengul, K. Sogut[24], B. Tali, H. Topakli, D. Uzun, L.N. Vergili, M. Vergili

Middle East Technical University, Physics Department, Ankara, Turkey
I.V. Akin, T. Aliev, S. Bilmis, M. Deniz, H. Gamsizkan, A.M. Guler, K. Öcalan, M. Serin, R. Sever, U.E. Surat, M. Zeyrek

Bogaziçi University, Department of Physics, Istanbul, Turkey
M. Deliomeroglu, D. Demir[25], E. Gülmez, A. Halu, B. Isildak, M. Kaya[26], O. Kaya[26], S. Ozkorucuklu[27], N. Sonmez[28]

National Scientific Center, Kharkov Institute of Physics and Technology, Kharkov, Ukraine
L. Levchuk

University of Bristol, Bristol, United Kingdom
P. Bell, F. Bostock, J.J. Brooke, T.L. Cheng, D. Cussans, R. Frazier, J. Goldstein, M. Hansen,

G.P. Heath, H.F. Heath, C. Hill, B. Huckvale, J. Jackson, L. Kreczko, C.K. Mackay, S. Metson, D.M. Newbold[29], K. Nirunpong, V.J. Smith, S. Ward

Rutherford Appleton Laboratory, Didcot, United Kingdom
L. Basso, K.W. Bell, C. Brew, R.M. Brown, B. Camanzi, D.J.A. Cockerill, J.A. Coughlan, K. Harder, S. Harper, B.W. Kennedy, C.H. Shepherd-Themistocleous, I.R. Tomalin, W.J. Womersley, S.D. Worm

Imperial College, University of London, London, United Kingdom
R. Bainbridge, G. Ball, J. Ballin, R. Beuselinck, O. Buchmuller, D. Colling, N. Cripps, G. Davies, M. Della Negra, C. Foudas, J. Fulcher, D. Futyan, G. Hall, J. Hays, G. Iles, G. Karapostoli, L. Lyons, B.C. MacEvoy, A.-M. Magnan, J. Marrouche, J. Nash, A. Nikitenko[21], A. Papageorgiou, M. Pesaresi, K. Petridis, M. Pioppi[30], D.M. Raymond, N. Rompotis, A. Rose, M.J. Ryan, C. Seez, P. Sharp, M. Stoye, A. Tapper, S. Tourneur, M. Vazquez Acosta, T. Virdee[1], S. Wakefield, D. Wardrope, T. Whyntie

Brunel University, Uxbridge, United Kingdom
M. Barrett, M. Chadwick, J.E. Cole, P.R. Hobson, A. Khan, P. Kyberd, D. Leslie, I.D. Reid, L. Teodorescu

Boston University, Boston, USA
T. Bose, A. Clough, A. Heister, J. St. John, P. Lawson, D. Lazic, J. Rohlf, L. Sulak

Brown University, Providence, USA
J. Andrea, A. Avetisyan, S. Bhattacharya, J.P. Chou, D. Cutts, S. Esen, G. Kukartsev, G. Landsberg, M. Narain, D. Nguyen, T. Speer, K.V. Tsang

University of California, Davis, Davis, USA
R. Breedon, M. Calderon De La Barca Sanchez, D. Cebra, M. Chertok, J. Conway, P.T. Cox, J. Dolen, R. Erbacher, E. Friis, W. Ko, A. Kopecky, R. Lander, H. Liu, S. Maruyama, T. Miceli, M. Nikolic, D. Pellett, J. Robles, M. Searle, J. Smith, M. Squires, M. Tripathi, R. Vasquez Sierra, C. Veelken

University of California, Los Angeles, Los Angeles, USA
V. Andreev, K. Arisaka, D. Cline, R. Cousins, S. Erhan[1], C. Farrell, J. Hauser, M. Ignatenko, C. Jarvis, G. Rakness, P. Schlein[†], J. Tucker, V. Valuev, R. Wallny

University of California, Riverside, Riverside, USA
J. Babb, A. Chandra, R. Clare, J.A. Ellison, J.W. Gary, G. Hanson, G.Y. Jeng, S.C. Kao, F. Liu, H. Liu, A. Luthra, H. Nguyen, B.C. Shen[†], R. Stringer, J. Sturdy, R. Wilken, S. Wimpenny

University of California, San Diego, La Jolla, USA
W. Andrews, J.G. Branson, E. Dusinberre, D. Evans, F. Golf, A. Holzner, R. Kelley, M. Lebourgeois, J. Letts, B. Mangano, J. Muelmenstaedt, M. Norman, S. Padhi, G. Petrucciani, H. Pi, M. Pieri, R. Ranieri, M. Sani, V. Sharma[1], S. Simon, A. Vartak, F. Würthwein, A. Yagil

University of California, Santa Barbara, Santa Barbara, USA
D. Barge, M. Blume, C. Campagnari, M. D'Alfonso, T. Danielson, J. Garberson, J. Incandela, C. Justus, P. Kalavase, S.A. Koay, D. Kovalskyi, V. Krutelyov, J. Lamb, S. Lowette, V. Pavlunin, F. Rebassoo, J. Ribnik, J. Richman, R. Rossin, D. Stuart, W. To, J.R. Vlimant, M. Witherell

California Institute of Technology, Pasadena, USA
A. Apresyan, A. Bornheim, J. Bunn, M. Gataullin, V. Litvine, Y. Ma, H.B. Newman, C. Rogan, V. Timciuc, J. Veverka, R. Wilkinson, Y. Yang, R.Y. Zhu

Carnegie Mellon University, Pittsburgh, USA
B. Akgun, R. Carroll, T. Ferguson, D.W. Jang, S.Y. Jun, M. Paulini, J. Russ, N. Terentyev, H. Vogel, I. Vorobiev

University of Colorado at Boulder, Boulder, USA
J.P. Cumalat, M.E. Dinardo, B.R. Drell, W.T. Ford, B. Heyburn, E. Luiggi Lopez, U. Nauenberg, K. Stenson, K. Ulmer, S.R. Wagner, S.L. Zang

Cornell University, Ithaca, USA
L. Agostino, J. Alexander, F. Blekman, D. Cassel, A. Chatterjee, S. Das, N. Eggert, L.K. Gibbons, B. Heltsley, W. Hopkins, A. Khukhunaishvili, B. Kreis, J.R. Patterson, D. Puigh, A. Ryd, X. Shi, W. Sun, W.D. Teo, J. Thom, J. Vaughan, Y. Weng, P. Wittich

Fairfield University, Fairfield, USA
A. Biselli, G. Cirino, D. Winn

Fermi National Accelerator Laboratory, Batavia, USA
M. Albrow, G. Apollinari, M. Atac, J.A. Bakken, S. Banerjee, L.A.T. Bauerdick, A. Beretvas, J. Berryhill, P.C. Bhat, M. Binkley†, I. Bloch, F. Borcherding, K. Burkett, J.N. Butler, V. Chetluru, H.W.K. Cheung, F. Chlebana, S. Cihangir, M. Demarteau, D.P. Eartly, V.D. Elvira, I. Fisk, J. Freeman, E. Gottschalk, D. Green, O. Gutsche, A. Hahn, J. Hanlon, R.M. Harris, E. James, H. Jensen, M. Johnson, U. Joshi, B. Klima, K. Kousouris, S. Kunori, S. Kwan, P. Limon, L. Lueking, J. Lykken, K. Maeshima, J.M. Marraffino, D. Mason, P. McBride, T. McCauley, T. Miao, K. Mishra, S. Mrenna, Y. Musienko[31], C. Newman-Holmes, V. O'Dell, S. Popescu, O. Prokofyev, E. Sexton-Kennedy, S. Sharma, R.P. Smith†, A. Soha, W.J. Spalding, L. Spiegel, P. Tan, L. Taylor, S. Tkaczyk, L. Uplegger, E.W. Vaandering, R. Vidal, J. Whitmore, W. Wu, F. Yumiceva, J.C. Yun

University of Florida, Gainesville, USA
D. Acosta, P. Avery, D. Bourilkov, M. Chen, G.P. Di Giovanni, D. Dobur, A. Drozdetskiy, R.D. Field, Y. Fu, I.K. Furic, J. Gartner, B. Kim, S. Klimenko, J. Konigsberg, A. Korytov, K. Kotov, A. Kropivnitskaya, T. Kypreos, K. Matchev, G. Mitselmakher, Y. Pakhotin, J. Piedra Gomez, C. Prescott, V. Rapsevicius, R. Remington, M. Schmitt, B. Scurlock, D. Wang, J. Yelton, M. Zakaria

Florida International University, Miami, USA
C. Ceron, V. Gaultney, L. Kramer, L.M. Lebolo, S. Linn, P. Markowitz, G. Martinez, J.L. Rodriguez

Florida State University, Tallahassee, USA
T. Adams, A. Askew, J. Chen, W.G.D. Dharmaratna, B. Diamond, S.V. Gleyzer, J. Haas, S. Hagopian, V. Hagopian, M. Jenkins, K.F. Johnson, H. Prosper, S. Sekmen

Florida Institute of Technology, Melbourne, USA
M.M. Baarmand[32], S. Guragain, M. Hohlmann, H. Kalakhety, H. Mermerkaya, R. Ralich, I. Vodopiyanov

University of Illinois at Chicago (UIC), Chicago, USA
M.R. Adams, I.M. Anghel, L. Apanasevich, V.E. Bazterra, R.R. Betts, J. Callner, R. Cavanaugh, C. Dragoiu, E.J. Garcia-Solis, C.E. Gerber, D.J. Hofman, S. Khalatian, C. Mironov, E. Shabalina, A. Smoron, N. Varelas

The University of Iowa, Iowa City, USA
U. Akgun, E.A. Albayrak, B. Bilki, K. Cankocak[33], K. Chung, W. Clarida, F. Duru, C.K. Lae,

E. McCliment, J.-P. Merlo, A. Mestvirishvili, A. Moeller, J. Nachtman, C.R. Newsom, E. Norbeck, J. Olson, Y. Onel, F. Ozok, S. Sen, J. Wetzel, T. Yetkin, K. Yi

Johns Hopkins University, Baltimore, USA
B.A. Barnett, B. Blumenfeld, A. Bonato, C. Eskew, D. Fehling, G. Giurgiu, A.V. Gritsan, Z.J. Guo, G. Hu, P. Maksimovic, S. Rappoccio, M. Swartz, N.V. Tran

The University of Kansas, Lawrence, USA
P. Baringer, A. Bean, G. Benelli, O. Grachov, M. Murray, V. Radicci, S. Sanders, J.S. Wood, V. Zhukova

Kansas State University, Manhattan, USA
D. Bandurin, A.F. Barfuss, T. Bolton, I. Chakaberia, K. Kaadze, Y. Maravin, S. Shrestha, I. Svintradze, Z. Wan

Lawrence Livermore National Laboratory, Livermore, USA
J. Gronberg, D. Lange, D. Wright

University of Maryland, College Park, USA
D. Baden, M. Boutemeur, S.C. Eno, D. Ferencek, N.J. Hadley, R.G. Kellogg, M. Kirn, K. Rossato, P. Rumerio, F. Santanastasio, A. Skuja, J. Temple, M.B. Tonjes, S.C. Tonwar, E. Twedt

Massachusetts Institute of Technology, Cambridge, USA
B. Alver, G. Bauer, J. Bendavid, W. Busza, E. Butz, I.A. Cali, M. Chan, D. D'Enterria, P. Everaerts, G. Gomez Ceballos, M. Goncharov, K.A. Hahn, P. Harris, Y. Kim, M. Klute, Y.-J. Lee, W. Li, C. Loizides, P.D. Luckey, T. Ma, S. Nahn, C. Paus, C. Roland, G. Roland, M. Rudolph, G.S.F. Stephans, K. Sumorok, K. Sung, E.A. Wenger, B. Wyslouch, S. Xie, Y. Yilmaz, A.S. Yoon, M. Zanetti

University of Minnesota, Minneapolis, USA
P. Cole, S.I. Cooper, P. Cushman, B. Dahmes, A. De Benedetti, P.R. Dudero, G. Franzoni, J. Haupt, K. Klapoetke, Y. Kubota, J. Mans, D. Petyt, V. Rekovic, R. Rusack, M. Sasseville, A. Singovsky

University of Mississippi, University, USA
L.M. Cremaldi, R. Godang, R. Kroeger, L. Perera, R. Rahmat, D.A. Sanders, P. Sonnek, D. Summers

University of Nebraska-Lincoln, Lincoln, USA
K. Bloom, S. Bose, J. Butt, D.R. Claes, A. Dominguez, M. Eads, J. Keller, T. Kelly, I. Kravchenko, J. Lazo-Flores, C. Lundstedt, H. Malbouisson, S. Malik, G.R. Snow

State University of New York at Buffalo, Buffalo, USA
U. Baur, I. Iashvili, A. Kharchilava, A. Kumar, K. Smith, M. Strang

Northeastern University, Boston, USA
G. Alverson, E. Barberis, D. Baumgartel, O. Boeriu, S. Reucroft, J. Swain, D. Wood

Northwestern University, Evanston, USA
A. Anastassov, A. Kubik, R.A. Ofierzynski, A. Pozdnyakov, M. Schmitt, S. Stoynev, M. Velasco, S. Won

University of Notre Dame, Notre Dame, USA
L. Antonelli, D. Berry, M. Hildreth, C. Jessop, D.J. Karmgard, J. Kolb, T. Kolberg, K. Lannon, S. Lynch, N. Marinelli, D.M. Morse, R. Ruchti, N. Valls, J. Warchol, M. Wayne, J. Ziegler

The Ohio State University, Columbus, USA
B. Bylsma, L.S. Durkin, J. Gu, P. Killewald, T.Y. Ling, G. Williams

Princeton University, Princeton, USA
N. Adam, E. Berry, P. Elmer, D. Gerbaudo, V. Halyo, A. Hunt, J. Jones, E. Laird, D. Lopes Pegna, D. Marlow, T. Medvedeva, M. Mooney, J. Olsen, P. Piroué, D. Stickland, C. Tully, J.S. Werner, A. Zuranski

University of Puerto Rico, Mayaguez, USA
J.G. Acosta, X.T. Huang, A. Lopez, H. Mendez, S. Oliveros, J.E. Ramirez Vargas, A. Zatzerklyaniy

Purdue University, West Lafayette, USA
E. Alagoz, V.E. Barnes, G. Bolla, L. Borrello, D. Bortoletto, A. Everett, A.F. Garfinkel, Z. Gecse, L. Gutay, M. Jones, O. Koybasi, A.T. Laasanen, N. Leonardo, C. Liu, V. Maroussov, P. Merkel, D.H. Miller, N. Neumeister, K. Potamianos, A. Sedov, I. Shipsey, D. Silvers, H.D. Yoo, Y. Zheng

Purdue University Calumet, Hammond, USA
P. Jindal, N. Parashar

Rice University, Houston, USA
V. Cuplov, K.M. Ecklund, F.J.M. Geurts, J.H. Liu, M. Matveev, J. Morales, B.P. Padley, R. Redjimi, J. Roberts

University of Rochester, Rochester, USA
B. Betchart, A. Bodek, Y.S. Chung, P. de Barbaro, R. Demina, H. Flacher, A. Garcia-Bellido, Y. Gotra, J. Han, A. Harel, S. Korjenevski, D.C. Miner, D. Orbaker, G. Petrillo, D. Vishnevskiy, M. Zielinski

The Rockefeller University, New York, USA
A. Bhatti, L. Demortier, K. Goulianos, K. Hatakeyama[34], G. Lungu, C. Mesropian, M. Yan

Rutgers, the State University of New Jersey, Piscataway, USA
O. Atramentov, Y. Gershtein, E. Halkiadakis, D. Hits, A. Lath, K. Rose, S. Schnetzer, S. Somalwar, R. Stone, S. Thomas

University of Tennessee, Knoxville, USA
G. Cerizza, M. Hollingsworth, S. Spanier, Z.C. Yang, A. York

Texas A&M University, College Station, USA
J. Asaadi, R. Eusebi, J. Gilmore, A. Gurrola, T. Kamon, V. Khotilovich, C.N. Nguyen, J. Pivarski, A. Safonov, S. Sengupta, D. Toback, M. Weinberger

Texas Tech University, Lubbock, USA
N. Akchurin, C. Jeong, S.W. Lee, Y. Roh, A. Sill, I. Volobouev, R. Wigmans, E. Yazgan

Vanderbilt University, Nashville, USA
E. Brownson, D. Engh, C. Florez, W. Johns, P. Kurt, P. Sheldon

University of Virginia, Charlottesville, USA
M.W. Arenton, M. Balazs, M. Buehler, S. Conetti, B. Cox, R. Hirosky, A. Ledovskoy, C. Neu, R. Yohay

Wayne State University, Detroit, USA
S. Gollapinni, K. Gunthoti, R. Harr, P.E. Karchin, M. Mattson

University of Wisconsin, Madison, USA
M. Anderson, M. Bachtis, J.N. Bellinger, D. Carlsmith, S. Dasu, J. Efron, K. Flood, L. Gray, K.S. Grogg, M. Grothe, R. Hall-Wilton[1], P. Klabbers, J. Klukas, A. Lanaro, C. Lazaridis, J. Leonard, D. Lomidze, R. Loveless, A. Mohapatra, D. Reeder, A. Savin, W.H. Smith, J. Swanson, M. Weinberg

†: Deceased
1: Also at CERN, European Organization for Nuclear Research, Geneva, Switzerland
2: Also at Universidade Federal do ABC, Santo Andre, Brazil
3: Also at Université de Haute-Alsace, Mulhouse, France
4: Also at Centre de Calcul de l'Institut National de Physique Nucleaire et de Physique des Particules (IN2P3), Villeurbanne, France
5: Also at Moscow State University, Moscow, Russia
6: Also at Institute of Nuclear Research ATOMKI, Debrecen, Hungary
7: Also at University of California, San Diego, La Jolla, USA
8: Also at Tata Institute of Fundamental Research - HECR, Mumbai, India
9: Also at University of Visva-Bharati, Santiniketan, India
10: Also at Facolta' Ingegneria Università di Roma "La Sapienza", Roma, Italy
11: Also at Università della Basilicata, Potenza, Italy
12: Also at Laboratori Nazionali di Legnaro dell' INFN, Legnaro, Italy
13: Also at California Institute of Technology, Pasadena, USA
14: Also at Faculty of Physics of University of Belgrade, Belgrade, Serbia
15: Also at Laboratoire Leprince-Ringuet, Ecole Polytechnique, IN2P3-CNRS, Palaiseau, France
16: Also at Université de Genève, Geneva, Switzerland
17: Also at Scuola Normale e Sezione dell' INFN, Pisa, Italy
18: Also at University of Athens, Athens, Greece
19: Also at Eötvös Loránd University, Budapest, Hungary
20: Also at The University of Kansas, Lawrence, USA
21: Also at Institute for Theoretical and Experimental Physics, Moscow, Russia
22: Also at Paul Scherrer Institut, Villigen, Switzerland
23: Also at Vinca Institute of Nuclear Sciences, Belgrade, Serbia
24: Also at Mersin University, Mersin, Turkey
25: Also at Izmir Institute of Technology, Izmir, Turkey
26: Also at Kafkas University, Kars, Turkey
27: Also at Suleyman Demirel University, Isparta, Turkey
28: Also at Ege University, Izmir, Turkey
29: Also at Rutherford Appleton Laboratory, Didcot, United Kingdom
30: Also at INFN Sezione di Perugia; Università di Perugia, Perugia, Italy
31: Also at Institute for Nuclear Research, Moscow, Russia
32: Also at Institute for Studies in Theoretical Physics & Mathematics (IPM), Tehran, Iran
33: Also at Istanbul Technical University, Istanbul, Turkey
34: Also at Baylor University, Waco, USA